



**SYNTHESIS AND CHARACTERIZATION OF
 $\text{Ni}_{0.8}\text{Co}_{0.2}\text{Mn}_x\text{Fe}_{2-x}\text{O}_4$ NANO CRYSTALLINE FERRITE
MATERIALS**

**MSC THESIS
BY
GEZAHEGN GEZMU**

**OCTOBER, 2017
ARBA MINCH, ETHIOPIA**

**SYNTHESIS AND CHARACTERIZATION OF $\text{Ni}_{0.8}\text{Co}_{0.2}\text{Mn}_x\text{Fe}_{2-x}\text{O}_4$
NANO CRYSTALLINE FERRITE MATERIALS**

BY

GEZAHEGN GEZMU

UNDER THE GUIDANCE

OF

PAULOS TADESSE (PhD)

**A THESIS SUBMITTED TO THE DEPARTMENT OF PHYSICS, PARTIAL
FULFILLMENT OF THE REQUIREMENTS FOR THE DEGREE OF MASTERS OF
SCIENCE IN PHYSICS**

**OCTOBER, 2017
ARBA MINCH, ETHIOPIA**

DECLARATION

I, hereby declare that the work presented in the report entitled **“synthesis and characterization of $\text{Ni}_{0.8}\text{Co}_{0.2}\text{Mn}_x\text{Fe}_{2-x}\text{O}_4$ Nano crystalline ferrite materials”** is the original work done by me and has not been presented for degree of Masters in any other University and all sources of information used for the thesis have been fully acknowledged and has been done independently in the Department of physics, College of Natural sciences, Arba Minch University.

Name Gezahegn Gezmu

Date **October**/2017

Signature-----

Place Arba Minch University, Ethiopia

ARBA MINCH UNIVERSITY
SCHOOL OF GRADUATE STUDIES
ADVISORS' THESIS SUBMISSION APPROVAL SHEET

This is to certify that the thesis entitled “**Synthesis and characterization of $\text{Ni}_{0.8}\text{Co}_{0.2}\text{Mn}_x\text{Fe}_{2-x}\text{O}_4$ Nano crystalline ferrite materials**” submitted in partial fulfillment of the requirements for the degree of **Master in Pure Physics**, to the Graduate Program of the **Department of Physics**, and has been carried out by **Gezahegn Gezmu** Id. No **SMSc/130/06**, under my supervision. Therefore, I recommend that the student has fulfilled the requirements and hence hereby can submit the thesis to the department for defense.

Paulos Tadesse (PhD)

Name of Principal Advisor

Signature

Date

ARBA MINCH UNIVERSITY
SCHOOL OF GRADUATE STUDIES
EXAMINERS' THESIS APPROVAL SHEET

We, the undersigned, members of the Board of Examiners of the final open defense by Gezahegn Gezmu have read and evaluated his/her thesis entitled "Synthesis and characterization of $\text{Ni}_{0.8}\text{Co}_{0.2}\text{Mn}_x\text{Fe}_{2-x}\text{O}_4$ (where $x = 0.05$ and 0.1) Nano crystalline ferrite materials", and examined the candidate's oral presentation. This is, therefore, to certify that the thesis has been accepted in partial fulfillment of the requirements for the degree with **minor/major corrections**.

_____	_____	_____
Name of the Chairperson	Signature	Date
_____	_____	_____
Name of Advisor	Signature	Date
_____	_____	_____
Name of internal examiner	Signature	Date
_____	_____	_____
Name of External examiner	Signature	Date
_____	_____	_____
SGS Approval	Signature	Date

ACKNOWLEDGEMENTS

First of all I would like to thank the almighty God for his help throughout my life and accomplishment of this research work. With great pleasure, I would like to express my sincere and profound sense of gratitude to my advisor Dr. Paulos Tadesse for the encouragement and understanding throughout the period of this research work. It is with all sincerity and high regards that I state my obligation to Arba Minch University Department of Physics College of Natural Sciences for their constant encouragement and timely suggestions throughout the period. I would like to extend my special word of thanks to all my colleagues.

I would like to thank my wife w/ro Kelemuwa Mehammud and My Son Samuel for their immense moral support rendered to me in times of shade. Next, I would like to thank my father Ato Gezmu Geze and my Mother w/ro Alemitu Abate for their moral and financial support in doing and accomplishing my research work.

I would also like to thank Konta administrative office Head Ato Tesfaye Mekurya and Ato Markos Bulcha who, with their lifelong time knowledge and experience, opened a window for a successful student to peep into a research Work. Their unlimited idea and advice transformed me from a naive youth into a scientific thinker and researcher.

Finally, I would like to thank Arba Minch University for Financial and material support.

LIST OF ABBREVIATIONS AND SYMBOLS

CIS	Complex Impedance Spectroscopy
EDS	Energy Dispersive Spectroscopy
EDX	Energy Dispersive X-Ray
ESR	Electron Spin Resonance
FT-IR	Fourier Transforms Infrared
H_c	Coercivity
M_r	Remnant Magnetization
M_s	Saturation Magnetization
PVA	Polyvinyl Alcohol
SEM	Scanning Electron Microscopy
XRD	X-ray Diffraction
σ_{ac}	Alternating current conductivity
σ_{dc}	Direct current conductivity
$\tan\delta$	Dielectric loss

TABLE OF CONTENTS

ACKNOWLEDGEMENTS	V
LIST OF ABBREVIATIONS AND SYMBOLS	VI
LIST OF FIGURES	IX
ABSTRACT.....	X
CHAPTER ONE: INTRODUCTION.....	1
1.1 Background of the study	1
1.2 Statement of the problem.....	2
1.3 Objectives of the study.....	2
1.3.1 General objective.....	2
1.3.2 Specific objectives.....	2
1.4 Significance of the study.....	3
1.5 Scope of the present work	3
1.6 Thesis organization.....	4
CHAPTER TWO: LITERATURE REVIEW.....	5
2.1 General introduction.....	5
2.2 Ferrite Materials	6
2.2.1 Hard ferrites.....	6
2.2.2 Soft ferrites	7
2.3 Types of ferrites.....	7
2.3.1 Spinel ferrites	7
2.3.1.1 Normal spinel ferrites	8
2.3.1.2 Inverse spinel ferrite	9
2.3.1.3 Intermediate spinel ferrite.....	10
2.3.2 Hexagonal ferrite.....	10
2.3.3 Garnet	12
2.4 Application of ferrites	13
2.5 Material synthesis methods	14
2.5.1 Solis state Reaction synthesis.....	14

2.5.2 Sol-gel Synthesis	14
2.5.3 Sol-gel auto-combustion Synthesis	15
2.5.4 Hydrothermal Synthesis	17
CHAPTER THREE: METHODOLOGY OF THE STUDY	19
3.1 List of raw materials.....	19
3.2 Materials synthesis	19
3.3 Experimental procedures	20
3.3.1 Powder preparation	20
3.3.2 Pellet preparation for electrical characterization.....	22
3.4 Characterization techniques	23
3.4.1 X-ray Powder Diffraction.....	23
3.4.2 Scanning Electron Microscopy	25
3.4.3 Energy dispersive X-Ray spectroscopy.....	25
3.4.4 Fourier transform infrared spectroscopy	26
3.4.5 Complex impedance spectroscopy	26
3.4.6 Electron spins resonance spectroscopy	28
CHAPTER FOUR: RESULT AND DISCUSION	29
4.1 XRD analysis.....	29
4.2 SEM and EDS Studies.....	31
4.3 FT-IR Analysis	34
4.4 Electrical and dielectric properties studies	35
4.4.1 Variation of conductivity with frequency	35
4.4.2 Variation dielectric constant with frequency	36
4.5 Magnetic properties study	37
CHAPTER FIVE: CONCLUSION AND RECOMMENDATION	40
5.1 Conclusion.....	40
5.2 Recommendation.....	41
REFERENCES	42

LIST OF FIGURES

Figure 2.1 Crystal structure of unit cell of spinel ferrite	8
Figure 2.2 Cation distributions in inverse spinel ferrite.....	9
Figure 2.3 Cation distributions in Intermediate spinel ferrite	10
Figure 2.4 Ternary diagram showing the composition of the main barium hexagonal ferrites.....	11
Figure 2.5 Schematic representation of an ‘octant’ of a garnet crystal structure (Lattice constant ‘a’) showing cation positions.....	12
Figure 2.6 Steps in the sol-gel synthesis route.....	15
Figure 2.7 Combustion reaction of reactant mixture.....	16
Figure 3.1 Flow diagram of samples preparation.....	21
Figure 3.2 Flow chart of pellet preparation.....	23
Figure 4.1 Powder XRD patterns of $\text{Ni}_{0.8}\text{Co}_{0.2}\text{Mn}_{0.05}\text{Fe}_{1.95}\text{O}_4$ & $\text{Ni}_{0.8}\text{Co}_{0.2}\text{Mn}_{0.1}\text{Fe}_{1.9}\text{O}_4$ ferrite	30
Figure 4.2 SEM images of (a) $\text{Ni}_{0.8}\text{Co}_{0.2}\text{Mn}_{0.05}\text{Fe}_{1.95}\text{O}_4$ & (b) $\text{Ni}_{0.8}\text{Co}_{0.2}\text{Mn}_{0.1}\text{Fe}_{1.9}\text{O}_4$ ferrite.....	32
Figure 4.3 (a) EDX spectra and elemental analysis for (a) $\text{Ni}_{0.8}\text{Co}_{0.2}\text{Mn}_{0.05}\text{Fe}_{1.95}\text{O}_4$ & (b) $\text{Ni}_{0.8}\text{Co}_{0.2}\text{Mn}_{0.1}\text{Fe}_{1.9}\text{O}_4$ ferrite materials	33
Figure 4.4 FT-IR spectra of (a) $\text{Ni}_{0.8}\text{Co}_{0.2}\text{Mn}_{0.05}\text{Fe}_{1.95}\text{O}_4$ and (b) $\text{Ni}_{0.8}\text{Co}_{0.2}\text{Mn}_{0.1}\text{Fe}_{1.9}\text{O}_4$ ferrites.....	34
Figure 4.5 Variation of conductivity with frequency of (a) $\text{Ni}_{0.8}\text{Co}_{0.2}\text{Mn}_{0.05}\text{Fe}_{1.95}\text{O}_4$ and (b) $\text{Ni}_{0.8}\text{Co}_{0.2}\text{Mn}_{0.1}\text{Fe}_{1.9}\text{O}_4$ ferrites.....	36
Figure 4.6 Variation of dielectric constant ϵ' with frequency of (a) $\text{Ni}_{0.8}\text{Co}_{0.2}\text{Mn}_{0.05}\text{Fe}_{1.95}\text{O}_4$ and (b) $\text{Ni}_{0.8}\text{Co}_{0.2}\text{Mn}_{0.1}\text{Fe}_{1.9}\text{O}_4$ ferrites.....	37
Figure 4.7 Magnetic hysteresis loops for (a) $\text{Ni}_{0.8}\text{Co}_{0.2}\text{Mn}_{0.05}\text{Fe}_{1.95}\text{O}_4$ and (b) $\text{Ni}_{0.8}\text{Co}_{0.2}\text{Mn}_{0.1}\text{Fe}_{1.9}\text{O}_4$ nanoferrite at room temperature.....	38

ABSTRACT

Nano sized $\text{Ni}_{0.8}\text{Co}_{0.2}\text{Mn}_x\text{Fe}_{2-x}\text{O}_4$ ferrites with varies compositions ($x = 0.05$ and 0.1) are successfully synthesized by Sol–gel auto combustion method. The structure, morphology, chemical composition, electrical, dielectric and magnetic properties of these synthesized samples are investigated using x-ray powder diffraction (XRD), scanning electron microscopy (SEM), energy dispersive X-Ray spectroscopy (EDS), Fourier transform infrared (FT-IR) spectroscopy, impedance analyzer (IR) as well as Electron spin resonance spectroscopy (ESR). The XRD analysis confirms the phase purity of the synthesized ferrites. It also reveals the formation of spinel structure for both prepared powder ferrites. The lattice parameter and the crystal size of are identified to be 8.538 \AA and 58.23 nm , respectively for $\text{Ni}_{0.8}\text{Co}_{0.2}\text{Mn}_{0.05}\text{Fe}_{1.95}\text{O}_4$ ferrite material; and 8.561 \AA and 59.14 nm , respectively for $\text{Ni}_{0.8}\text{Co}_{0.2}\text{Mn}_{0.1}\text{Fe}_{1.9}\text{O}_4$ ferrite material. The average crystallite size calculated using Debye–Scherer equation also confirms the nano crystalline nature of the samples.

EDS patterns confirm the compositional formation of the synthesized samples, i.e., both compounds show the presence of Ni, Co, Mn, Fe and O elements. FT-IR spectra analysis shows the appearance of two strong bands, which are responsible for the formation of cubic spinel structures in both ferrites. From the electrical conductivity study, two different regions, which are frequency independent and dependent regions, are clearly identified. The variation of dielectric properties with frequency shows the polarization behavior of both ferrites. ESR study shows that both ferrite materials possess soft magnetization behavior at room temperature. The magnetization curves of both samples show weak ferromagnetic behavior, with slender hysteresis.

CHAPTER ONE

INTRODUCTION

1.1 Background of the study

Spinel ferrites are a very important group of magnetic materials due to their remarkable electrical and magnetic properties and wide practical application to information storage system, Ferrofluid technology, magnetocaloric refrigeration, catalysis, and medical diagnostics [1]. Spinel ferrites have the general formula of MFe_2O_4 , where M usually represents one or more than one of the divalent transition metals Mn, Fe, Co, Ni, Cu, Zn, or other metals [2]. Among the spinel ferrites, the inverse type is particularly interesting due to its high magnetocrystalline anisotropy, high saturation magnetization, and unique magnetic structure [3].

Nowadays the synthesis of spinel ferrite nanoparticles has been intensively studied, because of their remarkable electrical and magnetic properties and wide practical application to information storage system [3]. These properties are dependent on chemical composition and microstructural characteristics, which can be controlled in the fabrication and synthesis processes. The principal role of the preparation conditions on the morphological and structural features of the ferrites have been discussed in several papers. Various methods of synthesizing spinel cobalt ferrite nanoparticles have been reported, such as solid-state reaction method, co-precipitation, hydrothermal and sol-gel methods [4].

Recently, a sol-gel auto-combustion method has attracted much attention due to its valuable advantages such as homogeneous reactant distribution and low processing temperature. The products obtained by this method exhibits high crystalline quality, enhanced homogeneity, better control for size, shape, and degree of agglomeration of the resulting nanocrystals, simple compositional control uniform shape [4].

The structure, morphology, electrical and magnetic properties of both samples are studied using x-ray powder diffraction (XRD), scanning electron microscopy (SEM), energy dispersive X-Ray spectroscopy (EDS), Fourier transform infrared (FT-IR) spectroscopy, impedance analyzer as well as Electron spin resonance spectroscopy.

1.2 Statement of the problem

Nickel ferrite (NiFe_2O_4) is an inverse spinel in which half of the ferric ions fill the tetrahedral sites and the rest occupy the octahedral sites. NiFe_2O_4 is used in applications including high density magnetic recording media, magnetic refrigeration, magnetic liquids, microwave absorber, and repulsive suspension for levitated railway systems. NiFe_2O_4 exhibits unusual physical and chemical properties when its size is reduced into the Nano level.

It is well known that the physical properties, such as the structure, electrical, dielectric and magnetic properties of the ferrite nanomaterials are strongly dependent on the method of preparation. To date a broad variety of techniques are successfully developed for synthesis of nanocrystalline ferrites such as sol-gel, co-precipitation, solid-state reaction and others. In view of the above, this research work focuses on the synthesis of Mn-substituted $\text{Ni}_{0.8}\text{Co}_{0.2}\text{Mn}_x\text{Fe}_{2-x}\text{O}_4$ nanoparticles ferrites by sol-gel auto-combustion method and study of their structural, electrical, dielectric, and magnetic properties to determine any possible change in their physical properties due to substitution effect. To our knowledge, nanocrystalline spinels $\text{Ni}_{0.8}\text{Co}_{0.2}\text{Mn}_{0.05}\text{Fe}_{1.95}\text{O}_4$ and $\text{Ni}_{0.8}\text{Co}_{0.2}\text{Mn}_{0.1}\text{Fe}_{1.9}\text{O}_4$ ferrites synthesized by sol-gel auto-combustion have not been yet reported.

1.3 Objectives

1.3.1 General objective

The general objective of this research work was to study the synthesis and characterizations of $\text{Ni}_{0.8}\text{Co}_{0.2}\text{Mn}_x\text{Fe}_{2-x}\text{O}_4$ (where $x = 0.05, 0.1$) nanocrystalline powder material synthesized by a sol-gel auto-combustion method.

1.3.2 Specific objectives

- To synthesize $\text{Ni}_{0.8}\text{Co}_{0.2}\text{Mn}_x\text{Fe}_{2-x}\text{O}_4$ (where $x = 0.05$ and 0.1) nanocrystalline powder materials by sol-gel auto-combustion method.
- To characterize $\text{Ni}_{0.8}\text{Co}_{0.2}\text{Mn}_x\text{Fe}_{2-x}\text{O}_4$ (where $x = 0.05, 0.1$) ferrites using XRD, FT-IR, SEM, EDS, CIS and ESR techniques.
- To study the structure, electrical, dielectric and magnetic properties of $\text{Ni}_{0.8}\text{Co}_{0.2}\text{Mn}_x\text{Fe}_{2-x}\text{O}_4$ (where $x = 0.05, 0.1$) nanoferrite materials.
- To estimate the lattice parameters, crystal volume, crystal size, ac conductivity, and dielectric constants of the synthesized samples.

1.4 Significance of the study

From the literature survey, it is concluded that structure, electrical and magnetic properties of NiFe_2O_4 ferrites are largely dependent on the particle size. The particle size can be brought to Nano scale by using appropriate synthesis method. In some cases, substituted cations also contribute in reducing the particle size. This will help in reducing the calcination and sintering temperature so that particle growth can be suppressed to keep within the Nano scale. Therefore, it is very interesting to study the effect of cations substitutions on structure, electrical and magnetic properties of NiFe_2O_4 system for fundamental research to broaden the idea of physical mechanism behind the cause $\text{Ni}_{0.8}\text{Co}_{0.2}\text{Mn}_x\text{Fe}_{2-x}\text{O}_4$ (where $x = 0.05, 0.1$). We hope that this study can provide strong scientific information for further study of the materials and similar materials.

1.5 Scope of the present work

NiFe_2O_4 exhibits unusual physical and chemical properties while the size is reduced to the Nano level. While various synthesis methods have been studied, an effective approach to synthesize ferrite powders with the desired characterization at a reasonable cost is still lacking. And due to the fact that synthesis processes and the characterization are closely related, and also that the fundamental mechanisms are not fully understood, a constancy of the relation between the characterization and their performance is still lacking. Thus, the scope of this study is to study the synthesis and characterizations of $\text{Ni}_{0.8}\text{Co}_{0.2}\text{Mn}_x\text{Fe}_{2-x}\text{O}_4$ (where $x = 0.05, 0.1$) nanocrystalline powder material synthesized by a sol-gel auto-combustion method. The synthesized nanoferrite materials are characterized by using the following instrumental techniques:

- X-ray Powder diffraction (XRD),
- Scanning electron microscopy (SEM),
- Energy dispersive X-ray analysis (EDS),
- Fourier transforms infrared (FT-IR) spectroscopy,
- Impedance analyzer and
- Electron spin resonance spectroscopy (ESR)

1.6 Thesis organization

This thesis begins with the introductory chapter that introduces the ideas that compelling the research conducted and outlines the research work undertaken to achieve the goal.

Chapter two gives a general review of ferrites and microstructural properties, economic benefits in the nanotechnology, its drawbacks and the brief explanation of sol-gel auto-combustion synthesis method.

List of materials, material synthesis, the method of preparation and experimental procedures employed to powder and pellet preparation, as well as different characterization techniques are described in **chapter three**.

Chapter four discusses results obtained from this research work, such as the structure, the morphology, the EDS spectra, the FT-IR study, the electrical, dielectric and magnetic properties of $\text{Ni}_{0.8}\text{Co}_{0.2}\text{Mn}_x\text{Fe}_{2-x}\text{O}_4$ (where $x = 0.05, 0.1$) ferrites. Finally, **chapter five** presents conclusions of the study and recommendations for future work.

CHAPTER TWO

LITERATURE REVIEW

2.1 General introduction

Research into the synthesis and properties of nanoscale materials has exploded over the past decade due to the unique size dependent properties of nanoparticles that often differ considerably from their bulk phase materials behave[5]. Nano powders have grains size of the order of 1-100 nm in at least one co-ordinate and normally in three. Nano powders owing to small size, nanoparticles show properties which are surprisingly different from those of bulk system and the atoms indicating how the bulk properties evolve from atomic properties [5].

Nanocomposite is defined as a material that contains a reinforcement component in the form of one or more ultra-fine phase with dimensions less than 100 nm [5]. They have reported nanocomposite approach has been used to prove various material properties including mechanical, chemical, structural, optical, electrical and magnetic properties.

The spinel ferrites (MFe_2O_4 , M is divalent cation) belong to an important class of magnetic materials because of their remarkable magnetic properties particularly in the radiofrequency region, physical flexibility, high electrical resistivity, mechanical hardness and chemical stability [6]. Magnetic properties in these ferrites can be tuned by choosing various kinds of M^+ divalent cations like Zn^{2+} , Mg^{2+} , Cu^{2+} and Ni^{2+} . They also have many applications of soft ferrites in various electronic devices [7]. The study of ionizing radiation effects in $MgAl_2O_4$ showing its high resistance to displaying radiation damage which makes it a good candidate for fusion technology applications [8]. Spinel ferrite is a very informative crystal system for understanding and designing the magnetic properties of nanoparticles through chemical manipulations. Many synthetic approaches have been employed to prepare spinel ferrite nanocrystals [9].

The wet chemical synthesis of high reactive powders has been proved to be one of the most effective routes to decrease the sintering temperature of ferrites [10]. A variety of chemical synthesis methods, sol-gel process [10], spray pyrolysis, micro emulsion technique and hydrothermal process [11] etc.; have been proposed for preparation of nanomaterials.

Many studies have been reported on the preparation of nickel and cobalt ferrites, and their advantages by sol-gel method. The key advantages offered by the sol-gel process are: inexpensive precursors, simple synthesis method, and low sintering temperature, control of chemical composite, and morphology and size distribution. Sol-gel auto combustion technique is a novel way with a unique combination of chemical sol-gel process and combustion process.

The selection of ferrites material for specific application mainly depends on the basic constituents of the composition [12]. Ferrites with spontaneous rectangular hysteresis loop behavior with high rectangularity ratio are widely used in switching devices. The transition temperature from ferromagnetism to Para magnetism decrease with addition of Mn cations in $\text{Co}_{1-x}\text{Mn}_x\text{Fe}_2\text{O}_4$ spinel ferrites [13]. The oxide based magnetic nanoparticles have been investigated by many researchers because of the interesting magnetic properties such as super paramagnetic relaxation, surface effect by spin-canted structure, magneto electrical transport and so on.

2.2 Ferrite Materials

A ferrite is a type of ceramic compound composed of iron (III) oxide (Fe_2O_3) combined chemically with one or more additional metallic elements [3]. They are an important class of magnetic materials which have many applications, ranging from radio frequency and microwave frequency. They are technologically important materials having both electrical and magnetic properties i.e. they are electrically nonconductive or electrical insulator and ferromagnetic, meaning they can be magnetized or attracted to a magnet. The molecular formula of ferrites is $\text{M}^{2+}\text{OFe}_2^{3+}\text{O}_3$; there M represents divalent transition metal such as Fe, Ni, Ti, Cr, Zr, Zn, Pd, Ba, etc. [14]. In terms of their magnetic coercivity and their resistance to being demagnetized; Ferrites can be divided into Hard and Soft ferrites.

2.2.1 Hard ferrites

Hard ferrites are known to be permanent ferrite magnets having high coercivity and high remnance after magnetization. They are composed of iron and barium or strontium oxides. In a magnetically saturated state, they conduct magnetic flux well and have a high magnetic permeability. This enables these ceramic magnets to store stronger magnetic fields than iron itself [14]. Hard ferrite consists of ceramic magnets which are cheap, and are

widely used in household products such as refrigerator magnets. The most common known hard ferrites are Strontium ferrite, $\text{SrFe}_{12}\text{O}_{19}$ ($\text{SrO}\cdot 6\text{Fe}_2\text{O}_3$), Barium ferrite, $\text{BaFe}_{12}\text{O}_{19}$ ($\text{BaO}\cdot 6\text{Fe}_2\text{O}_3$), Cobalt ferrite, CoFe_2O_4 ($\text{CoO}\cdot \text{Fe}_2\text{O}_3$), and etc. [15, 16].

2.2.2 Soft ferrites

Soft ferrites are ferrimagnetic materials with cubic crystal structure and they are characterized by the chemical formula $\text{MO}\cdot \text{Fe}_2\text{O}_3$, where M is transition metal ions like Iron, Nickel, Manganese or Zinc. They can be both easily magnetized and demagnetized, so that they can store or transfer magnetic energy in alternating or other changing wave forms (sine, pulse, square, etc.) [17]. At high frequency, soft metal ferrites simply cannot be used due to the eddy current losses [16]. Therefore, soft ferrites, which are ceramic insulators, are technologically used in telephone signal transmitters and have low coercivity (means that the material's magnetization can easily reverse direction without dissipating much energy (hysteresis losses) [15].

The most common soft ferrites are Manganese-zinc ferrite with the formula $\text{Mn}_x\text{Zn}_{(1-x)}\text{Fe}_2\text{O}_4$, Nickel-zinc ferrite with the formula $\text{Ni}_x\text{Zn}_{(1-x)}\text{Fe}_2\text{O}_4$, Copper-zinc ferrite with the formula $\text{Cu}_x\text{Zn}_{(1-x)}\text{Fe}_2\text{O}_4$, and any other combination or doping of transition metals with the mother compound of ferrites [18]. They are used in the electronics industry to make ferrite cores for inductors and transformers, and in various microwave components. Ferrite compounds have extremely low cost, being made of iron oxide (i.e. rusted iron). They are very stable and have high resistance to demagnetization [19].

2.3 Types of ferrites

2.3.1 Spinel ferrites

Spinel ferrites are described by the chemical formula AB_2O_4 in which A and B display tetrahedral and octahedral cation sites, respectively, and O indicates the oxygen anion site [20]. They are also called cubic ferrites. In spinel ferrites, the relatively large oxygen anions form a cubic close packing with $\frac{1}{2}$ of the octahedral and $\frac{1}{8}$ of the tetrahedral interstitial sites occupied by metal ions [20]. Spinel ferrites with the formula AB_2O_4 or where A^{II} represents a divalent metal cation such as Mn, Fe, Co, Ni, Cu, Zn, Cd, Mg, and Fe^{III} is the trivalent iron cation, have the same crystallographic structure as the mineral spinel (MgAl_2O_4) [15].

However, Fe^{3+} ions can be replaced by other trivalent ions like Al^{3+} , Cr^{3+} , Ga^{3+} etc. Fe^{3+} ions can also be replaced by combination of divalent and tetravalent ions [21].

Spinel ferrites are magnetically soft and they are alternative to metallic magnets such as Fe and layered Fe-Si alloys, but exhibit enhanced performance due to their outstanding magnetic properties. These types of ferrites have the properties such as high electrical resistivity and low magnetic losses. The two popular ceramic magnets; Nickel-Zinc ferrites and Manganese-Zinc ferrites are the major members of the spinel ferrite family. They have been interesting ceramic materials due to their high electrical resistivity, high magnetic permeability and possible modification of intrinsic properties over a wide spectrum [22].

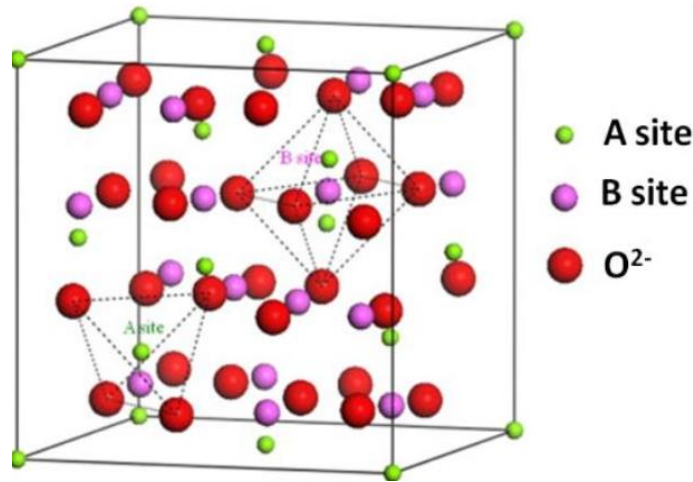


Figure 2.1 Crystal structure of unit cell of spinel ferrite [23].

According to the distribution of cations on tetrahedral (A) and octahedral (B) sites, spinel ferrites are classified into normal, inverse and intermediate (random) spinel ferrites.

2.3.1.1 Normal spinel ferrites

A material with the normal spinel structure having general formula $\text{M}(\text{Fe}_2)\text{O}_4$ has all the divalent metal (M) cations on the tetrahedral (A) sites and the trivalent (Fe) cations on the octahedral [B] sites. This can be represented by the formula $[\text{M}]_{\text{tet}}[\text{Fe}_2]_{\text{oct}}\text{O}_4$ [15]. In the mineral spinel, i.e. MgAl_2O_4 , the Mg^{2+} ions are in A sites and the Al^{3+} ions are in B sites. Some ferrites (Table 2.1) like $\text{MO}\cdot\text{Fe}_2\text{O}_3$ have exactly this structure, with M^{2+} in A sites and Fe^{3+} in B sites. Both zinc and cadmium ferrite have this structure and they are both nonmagnetic, i.e., paramagnetic [15, 24].

Table 2.1 List of some normal spinel ferrite

MgO.Al ₂ O ₃	MgAl ₂ O ₄	(normal, parent mineral)
ZnO.Fe ₂ O ₃	ZnFe ₂ O ₄	(normal)
FeO.Al ₂ O ₃	FeAl ₂ O ₄	(normal)
CoO.Al ₂ O ₃	CoAl ₂ O ₄	(normal)
MnO.Al ₂ O ₃	MnAl ₂ O ₄	(normal)
NiO.Al ₂ O ₃	NiAl ₂ O ₄	(normal)

2.3.1.2 Inverse spinel ferrite

In an inverse spinel structure, half of the trivalent cations are at the tetrahedral (A) site while the remaining trivalent ions and the divalent metallic ions M²⁺ are at the [B] site [15]. For example, cobalt ferrite (CoFe₂O₄) is predominantly an inverse spinel with a formula Co_xFe_{1-x}(Co_{1-x} Fe_{1+x})O₄ (with x = 0) where, x is the cation distribution factor which describes the fraction of tetrahedral sites occupied by Co²⁺ cations. Not all of the available sites are actually occupied by metal ions. Only one-eighth of the A sites and one-half of the B sites are occupied. In this type of spinel ferrites, the cations are distributed as shown in Figure 2.2.

Table 2.2 The Inverse spinel ferrites

CoO.Fe ₂ O ₃	FeCoFeO ₄	(Inverse)
NiO.Fe ₂ O ₃	FeNiFeO ₄	(Inverse)
MgO.Fe ₂ O ₃	FeMgFeO ₄	(Inverse)

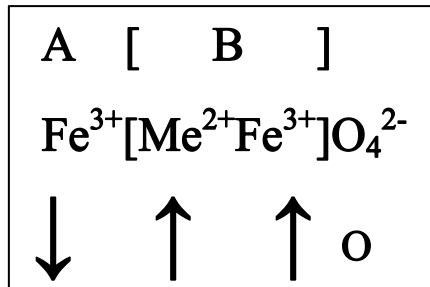


Figure 2.2 Cation distributions in inverse spinel ferrite.

2.3.1.3 Intermediate spinel ferrites

Intermediate spinel structures, which are also called mixed ferrites, are random spinels. The divalent and trivalent cations are randomly distributed on tetrahedral and octahedral sites. Random structures lie between normal spinel and inverse spinel. There is unequal number of cation on octahedral sites. Intermediate spinel ferrites are containing two or more different kinds of divalent ions, e.g. (Ni, Zn)O.Fe₂O₃ [15]. Most of the cubic ferrites used commercially are mixed ferrites. In random spinel ferrites, the M²⁺ and Fe³⁺ cations occupy both A and B sites. The cations distribution in this type of spinel ferrites is shown in Figure 2.3.

Generally, in spinel ferrites, if the divalent metal ions and trivalent Fe³⁺ ions are distributed randomly over the tetrahedral and octahedral B-sites, then the spinel ferrite is called random spinel [25].

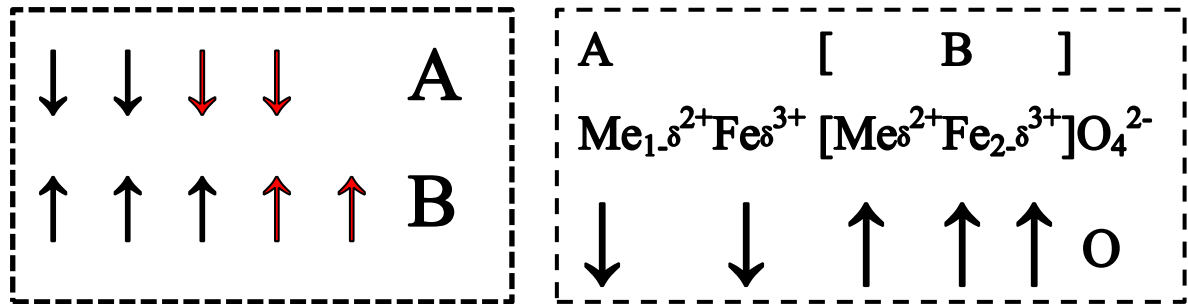


Figure 2.3 Cation distributions in Intermediate spinel ferrite.

2.3.2 Hexagonal ferrite

The group of ferrites possessing hexagonal crystal structure is referred to hexagonal ferrites. Six types of hexagonal ferrites are distinguished and indicated as M-type (BaFe₁₂O₁₉), W-type (BaMe₂Fe₁₆O₂₇), Y-type (Ba₂Me₂Fe₁₂O₂₂), X-type (Ba₂Me₂Fe₂₈O₄₆), Z-type (Ba₃Me₂Fe₂₄O₄₁) and U-type (Ba₄Me₂Fe₃₆O₆₀) [11] as shown in the composition diagram in Figure 2.4. They correspond to (MO + MeO)/Fe₂O₃ ratios of 1:6, 3:8, 4:6, 4:14, 5:12 and 6:18 respectively. Where M can be the ions Ba, Sr, Pb, Ca, La, etc. whilst Me is a transition cation (Zn, Mg, Mn, Co, etc.) or a combination of cations as it would occur in spinels. Moreover the substitution of Fe³⁺ with other trivalent cations such as Al³⁺, Ga³⁺, Sc³⁺, In³⁺ etc. is also possible. One can obtain an extremely large number of compounds with considerably

different magnetic properties. This fact makes the hexagonal ferrites attractive for different technical applications and interesting for basic studies on the magnetic interactions in insulators [26].

All of hexagonal ferrites are synthetic; the model compound of this family is barium Hexaferrites with formula $\text{BaFe}_{12}\text{O}_{19}$. Hexaferrites can also form an extensive variety of solid solutions. Ba can be substituted by Sr, Ca, and Pb. Fe^{3+} can be substituted by trivalent cations such as Al, Ga, by a combination of divalent and tetravalent cations, such as Co^{2+} and Ti^{4+} . Chemical substitution of B sites is usually done with Sr atoms while Fe atoms are substituted by Al atoms, based on the size and valence, resulting in a change in the magnetic behavior [27].

This was first identified by [28] that Hexaferrites are hexagonal or rhombohedra ferromagnetic oxides with formula $\text{MFe}_{12}\text{O}_{19}$, where M is an element like Barium, Lead or Strontium. In these ferrites, oxygen ions have closed packed hexagonal crystal structure. They are widely used as permanent magnets and have high coercivity. They are used at very high frequency. Their hexagonal ferrite lattice is similar to the spinel structure with closely packed oxygen ions, but there are also metal ions at some layers with the same ionic radii as that of oxygen ions. Hexagonal ferrites have larger ions than that of garnet ferrite and are formed by the replacement of oxygen ions. Most of these larger ions are barium, strontium or lead.

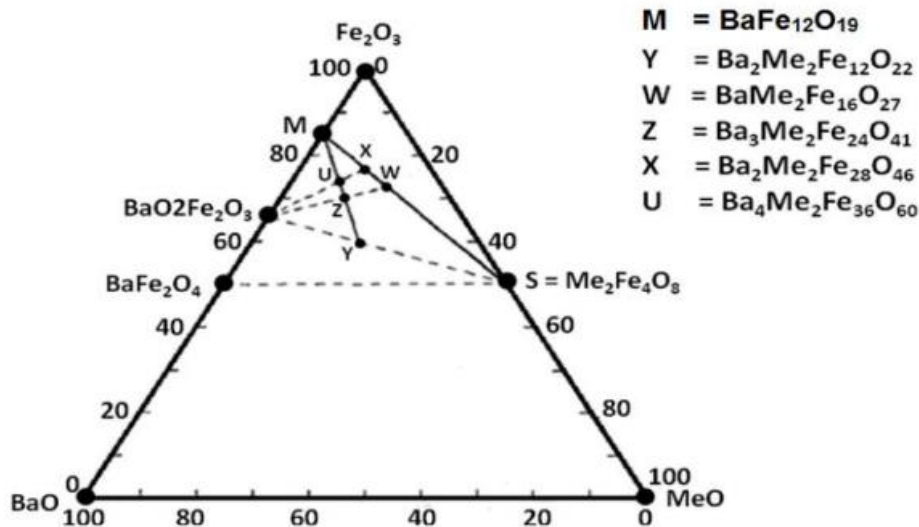


Figure 2. 4: Ternary diagram showing the composition of the main barium hexagonal ferrites [14].

2.3.3 Garnet

Garnets are a group of isomorphous minerals with a complex cubic structure. They have complex crystal structures. In the context of magnetic materials, garnets are represented by a general formula $Y_3Fe_5O_{12}$, containing two magnetic ions, one typically being iron and another being rare earth. Here R, in addition to yttrium can be one of lanthanide atoms such as lanthanum, cerium, samarium etc. [29].

Garnets can be quite useful materials in microwave applications because of their high electrical resistivity and hence lower losses around microwave frequencies. The material is also easy to synthesize in either of bulk polycrystalline ceramic, single crystal or thin film forms. The structural parameters as well as magnetic properties can be tuned by tailoring the composition of the material.

The unit cell of $Y_3Fe_5O_{12}$ has cubic symmetry crystal structure and contains 8 formula units i.e. 160 atoms, quite complex. In contrast with spinels, the oxygen sub lattice is not a close-packed arrangement, but it is better described as a polyhedral combination. Three kinds of cation sites exist in this structure: dodecahedral (eightfold), octahedral (six fold), and tetrahedral (four fold) sites. In garnet ferrites, orbital magnetic contribution of iron atoms is quenched due to shielding from crystal field while lanthanide ions contribute to both orbital and spin magnetic moment, thus contributing more to the total magnetic moment.

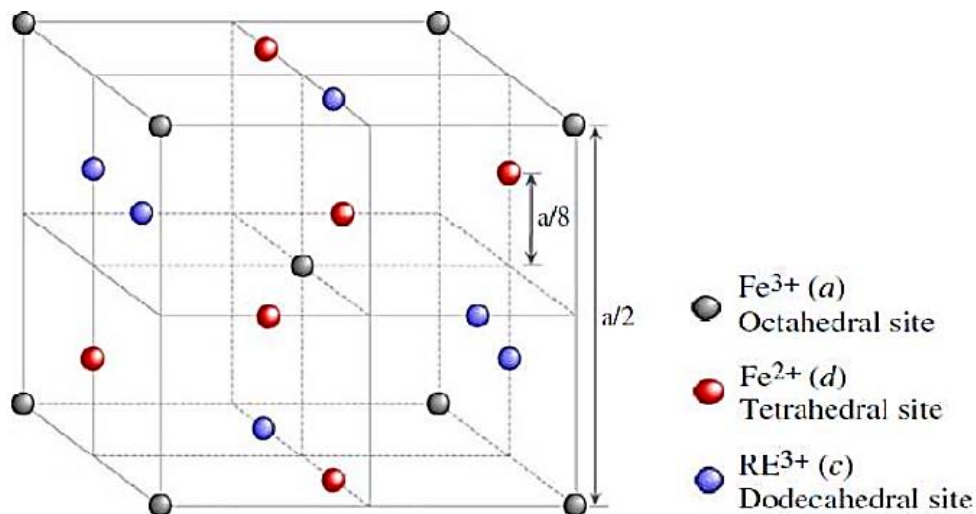


Figure 2.5 Schematic representation of an ‘octant’ of a garnet crystal structure (lattice constant ‘a’ showing cation position [30].

The general formula for garnets is $\text{Me}_3\text{Fe}_5\text{O}_{12}$, where Me is one of the rare earth metal ions, including Y, La and Gd. The cubic unit cell contains 8 formula units or 160 atoms, which can be described as a spatial arrangement of 96O^{2-} with interstitial cations. Yttrium iron garnet $\text{Y}_3\text{Fe}_5\text{O}_{12}$ (YIG) is a well-known garnet. The coordination of the cations is considerably more complex than spinels, with 24Y^{3+} in dodecahedral sites, 24Fe^{3+} ions in tetrahedral sites and 16 remaining Fe^{3+} in octahedral sites. Similar to spinels and hexagonal ferrites, a wide range of transition metal cations can substitute Y^{3+} or Fe^{3+} ; especially rare earth ions may replace the ions on octahedral and dodecahedral sites. Each type of lattice site will accept other metal ions at dodecahedral sites, octahedral sites and at tetrahedral sites. Thus pentavalent ions such as V^{5+} and As^{5+} can occupy tetrahedral sites, while Ca^{2+} substitute ions on dodecahedral sites [15].

2.4 Application of ferrites

The major commercial applications of ferrites in the technology are the following. They are used in medical diagnostic, science and industrial processing fields such as magnetic resonance imaging (MRI), nuclear magnetic resonance (NMR), High-energy physics accelerators, Plasma fusion reactors, industrial magnetic separation of kaolin clay materials and relatively high field magnets [31]. Indeed, without ferrites technology most of these applications would not be viable. Several smaller applications utilizing low temperature superconducting (LTS) materials have also been commercialized, e.g. research magnets and magneto encephalography (MEG). The latter is based on superconducting quantum interference device (SQUID) technology which detects and measures the weak magnetic fields generated by the brain [32].

Zero resistance and high current density have a major impact on electric power transmission and also enable much smaller or more powerful magnets for motors, generators, energy storage, medical equipment and industrial separations [3]. Low resistance at high frequencies [33] and extremely low signal dispersion are key aspects in microwave components, communications technology and several military applications [3,34,]. Magnetic field exclusion is important in multi-layer electronic component miniaturization, provides a mechanism for magnetic levitation and enables magnetic field containment of charged

particles. The final two properties form the basis for digital electronics and high speed computing well beyond the theoretical limits projected for semiconductors.

2.5 Material synthesis methods

2.5.1 Solid state reaction method

Solid state synthesis is one of the common methods employed for preparing powder materials from oxides, carbonates, hydroxides, nitrates, sulfates, and other metal salts [35]. The term solid-state synthesis process is often used to describe a chemical reaction between solids. In this method, solvents are not used. It involves heating mixtures of two or more solids to form a solid phase product. In solid state synthesis method, the reaction only occurs at contact points between the grains of the starting materials. Because of the very low diffusion coefficients in solids, the traditional solid-state synthesis requires high thermal activation and longer heating time than other techniques [34].

Advantages: Lower reaction temps, possibly stabilize metastable phases, the method can be used to prepare an extremely large number of compounds; it can be used to prepare a whole range of materials including mixed metal oxides, sulfides, nitrides, alumina silicates and eliminate intermediate impurity phases [34].

Disadvantages: long heating time to complete the reaction, can be hard to control exact stoichiometry in certain cases, and difficult control of stoichiometry the desired compound may decompose at high temperatures, the reaction may proceed very slowly, inhomogeneity, large particle size, agglomeration of the particles, irregular morphology, broad particle size distribution, difficult to incorporate ions that readily form volatile species, e.g.,(Ag⁺)[34].

2.5.2 Sol-gel synthesis

The sol-gel process is one of a wet chemical synthesis process to prepare ceramic and glass materials from nitrites, acetates, oxalates, etc. raw materials. The first investigation of a sol-gel process for synthesis was made in the mid-19th century. This early investigation studied the preparation of silica glass from a sol made by hydrolyzing an alkaoxides of silicon. The sol-gel method was further developed in the 1950s and 1960s after it was realized that colloids, which contain small particles (1–1000 nm in diameter), could be highly chemically homogeneous [36].

The sol-gel process involves transition from a liquid phase called sol into a gel phase. A sol is a colloidal suspension of particles in a liquid, which are 1 to 100 nm in diameter. A gel is a semi-rigid solid in which the solvent is contained in a framework of material which is either colloidal (essentially a concentrated sol) or polymeric. To prepare solids using the sol-gel method, first, a concentrated solution or colloidal suspension of the reactants, the 'sol', is prepared, which is then concentrated or matured to form the 'gel'. This homogeneous gel is then heat-treated to form the product. This heating serves several purposes: it removes the solvent, it decomposes anions such as alkoxides or carbonates to give oxides, it allows rearrangement of the structure of the solid, and it allows crystallization to occur. The main steps in the sol-gel process are outlined in Figure 2.6.

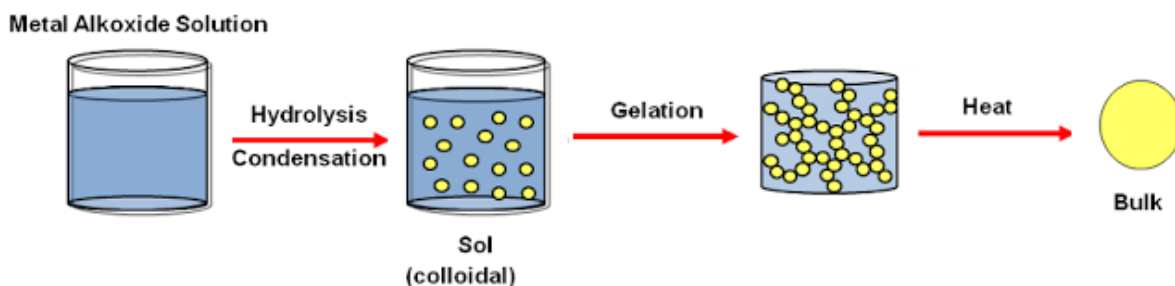


Figure 2.6 Steps in the sol-gel synthesis route [36]

The main advantages of sol-gel process are better homogeneity and purity, low temperature preparation, saving energy, minimize the evaporation losses, minimize air pollution, no reaction with container, bypass phase separation, etc. The disadvantages of the sol-gel process are: reaction may result with a wide particle size distribution, the composition of the obtained compounds may be inhomogeneous, expensive reagents are needed to perform the reaction, elevating operating temperatures are often required, and most of the procedures include a complicated preparation technique [37].

2.5.3 Sol-gel combustion synthesis

Combustion synthesis, also known as self-propagating high temperature synthesis, has been developed as an alternative route to the ceramic method which depends on the diffusion of ions through the reactants, and thus for a uniform product requires repeated heating and grinding for long periods [38]. Sol-gel combustion synthesis method (also called sol-gel self-combustion or sol-gel auto-combustion) where the chemical sol-gel and combustion process are

combined has shown great potential in the preparation of spinel type ferrite nanomaterials. Generally, this method can be considered as solution combustion technique and even explosive reactions to maintain a self-propagating high reaction temperature and has been used to prepare many refractory materials including borides, nitrides, oxides, silicide's, intermetallic, and ceramics. The reactants are mixed together, formed into a pellet, and then ignited (Figure 2.7) at high temperature.

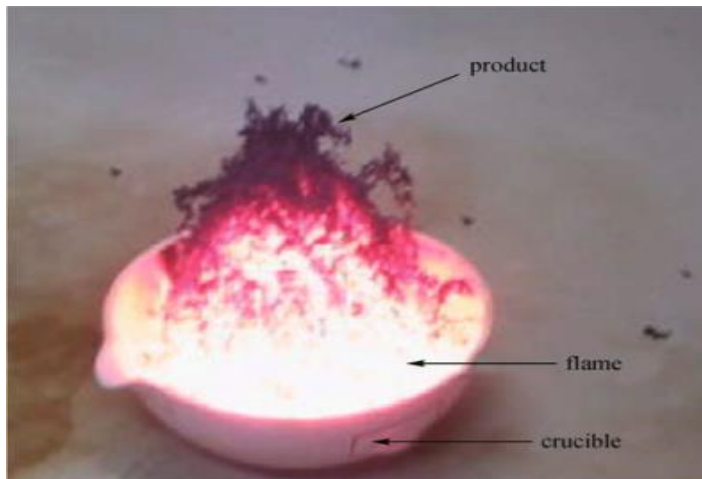


Figure2.7 Combustion reaction of reactant mixture [39].

Once ignited the reaction propagates as a wave, the synthesis wave, through the pellet, and the reaction must lose less heat than it generates or it will quench; temperatures up to 3000 K are maintained during the fast reactions[36].

Sol-gel auto-combustion synthesis technique plays a vital role in present day nanotechnology powder sample preparation. In this technique, oxidizing metal salts and combustion agent (fuel) are essential for the combustion process. Metal nitrates and citric acid were used as oxidizing salts and combustion fuel for all the sample preparations. All chemicals were of high purity analytical reagent and used without further purification [39, 40].

This method uses a solution during the initial step of the preparation process, so the reactants are well-dispersed and in a much higher reactive state, providing a homogeneous reaction mixture. The organic fuel plays an important role; it is the fuel for the combustion reaction; which forms complexes with metal ions preventing the precipitation of hydroxylated compounds [41]. The combustion can be considered as a thermally induced redox reaction.

The energy from the exothermic reaction between oxidant and reductant can be high enough to form fine particles [42].

Advantages of sol-gel auto-combustion process:-

Sol-gel auto-combustion methods show advantages over the other processes mainly due to the following important facts [43]:-

- Low cost and low temperature process,
- Better control of stoichiometry,
- Crystalline size of the final oxide products is invariably in the nanometer range,
- Exothermic reaction makes product almost instantaneously.
- Possibility of multicomponent oxides with single phase and high surface area,
- It can be performed relatively easily without using special equipment,
- It uses low energy consumption,
- It gives a homogeneous powder with a high level of purity and low particle size distribution,
- Fine particle size and narrow particle size distribution; it is easy to control stoichiometry,
- Simple equipment and preparation process; low processing time and
- low external energy consumption (process initiates at low temperatures) and multiple steps are not involved

Drawbacks of sol-gel auto combustion process [44]:-

- Contamination due to carbonaceous residue,
- Understanding of combustion behavior is needed to perform the controlled combustion in order to get final products with desired properties.

2.5.4 Hydrothermal Synthesis

Among the low temperature methods, the hydrothermal method is very versatile for the synthesis of Nano materials and has been well established. Although synthesis reactions can be carried out in a temperature range of 100 to 1000°C or more and in a pressure range of 1 atmosphere to several thousand atmospheres, most of the hydrothermal experiments are conducted below the supercritical temperature of water (374°C). The reactions can be carried

out in water or in any other solvent. When water is used as a solvent, the process is called 'hydrothermal processes and when any solvent including water or organic solvents such as methanol, ethanol, polyol, etc. are used, the process is termed 'solvothermal processes. Thus, the latter term encompasses all solvents including water. Nano phase oxides can be synthesized by the hydrothermal process.

The main advantages of the hydrothermal method are: kinetics of reaction are greatly increased with a small increase in temperature, single crystals are obtained, high purity products can be obtained, no precipitants are needed in many cases and thus the process is cost-effective, pollution is minimized because of the closed system conditions and reagents can be recycled, powders are formed directly from the solution, and possibility to control particle size and shapes by using different starting materials and hydrothermal conditions[45]. However, hydrothermal method has the following drawbacks: prior knowledge on solubility of starting materials is required, hydrothermal slurries are potentially corrosive and accidental explosion of the high pressure vessel cannot be ruled out [44, 46].

CHAPTER THREE

METHODS AND MATERIALS

3.1 List of raw materials

Chemicals which are required to be used in the study for synthesis and characterization of $\text{Ni}_{0.8}\text{Co}_{0.2}\text{Mn}_x\text{Fe}_{2-x}\text{O}_4$ (where $x = 0.05$ and 0.1) ferrite materials are shown in the Table 3.1.

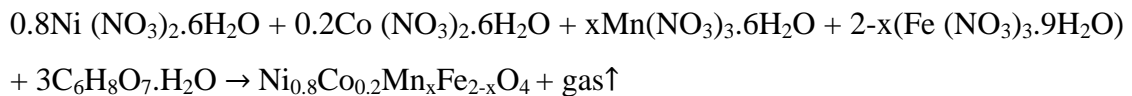
Table 3.1 List of chemicals and their formula.

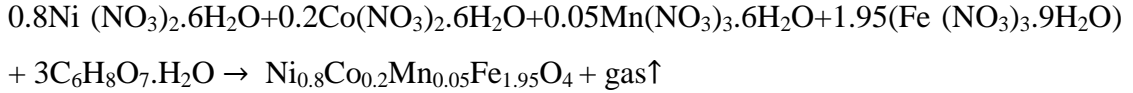
No	Chemicals	Chemical Formula
1	Nickel (II) nitrate Hexahydrate	$\text{Ni}(\text{NO}_3)_2 \cdot 6\text{H}_2\text{O}$
2	Iron(III) nitrate Nona hydrate	$\text{Fe}(\text{NO}_3)_3 \cdot 9\text{H}_2\text{O}$
3	Manganese (III) nitrate Hexahydrate	$\text{Mn}(\text{NO}_3)_3 \cdot 6\text{H}_2\text{O}$
4	Cobalt (II) nitrate Hexahydrate	$\text{Co}(\text{NO}_3)_2 \cdot 6\text{H}_2\text{O}$
5	Citric Acid Monohydrate	$\text{C}_6\text{H}_8\text{O}_7 \cdot \text{H}_2\text{O}$
6	Sulfuric Acid	H_2SO_4
7	Potassium Bromide	KBr
8	Silver	Ag
9	polyvinyl alcohol (PVA)	$(\text{C}_2\text{H}_3\text{OR})_n$
10	Ammonia hydroxide	NH_4OH

3.2 Materials synthesis

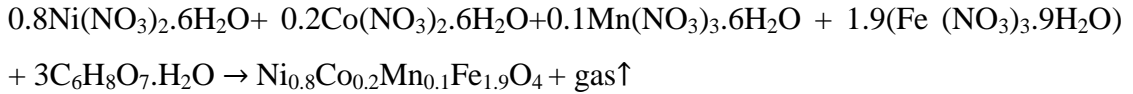
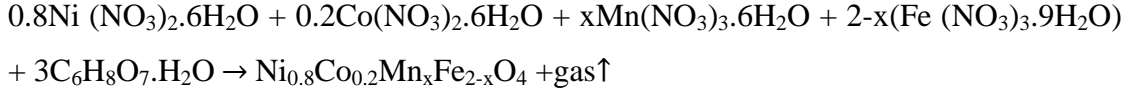
In this study, the following ferrite materials with typical formula are synthesized.

- $\text{Ni}_{0.8}\text{Co}_{0.2}\text{Mn}_{0.05}\text{Fe}_{1.95}\text{O}_4$





- **Ni_{0.8}Co_{0.2}Mn_{0.05}Fe_{1.95}O₄**



3.3 Experimental procedures

3.3.1 Powder preparation

Ni_{0.8}Co_{0.2}Mn_xFe_{2-x}O₄ (x = 0.05 and 0.1) ferrites are synthesized by sol-gel auto-combustion reaction method using Ni(NO₃)₂·6H₂O, Fe(NO₃)₃·9H₂O, Co(NO₃)₂·6H₂O and Mn(NO₃)₃·6H₂O and C₆H₈O₇·H₂O as starting material. Stoichiometric amounts of Ni(NO₃)₂·6H₂O, Fe(NO₃)₃·9H₂O, Co(NO₃)₂·6H₂O and Mn(NO₃)₃·6H₂O and C₆H₈O₇·H₂O are dissolved in some amount of de-ionized water. Aqueous ammonia solution is then added drop by drop under constant stirring using magnetic stirrer until the pH value maintained about 7. This mixed solution is constantly stirred by magnetic stirrer on a hot plate at 80°C for 4 hours in the water bath and stirred continuously until to obtain a dark brown gel. When the obtained gel was heated at 200 °C inside oven, auto-combustion process was started in the hottest zones of the beaker and propagated to self-ignition from the bottom to the top like the eruption of a volcano, the gel completely burnt out to form a powder. Further, the obtained powder was ground in an agate mortar for about 1 hrs. After thorough homogenizing, the powder materials are heated at 700 °C for 5 hrs in the electric furnace. Finally, Ni_{0.8}Co_{0.2}Mn_{0.05}Fe_{1.95}O₄ and Ni_{0.8}Co_{0.2}Mn_{0.1}Fe_{1.9}O₄ materials in the form of powder are obtained. The detail of the synthesis process is shown in figure 3.1 below.

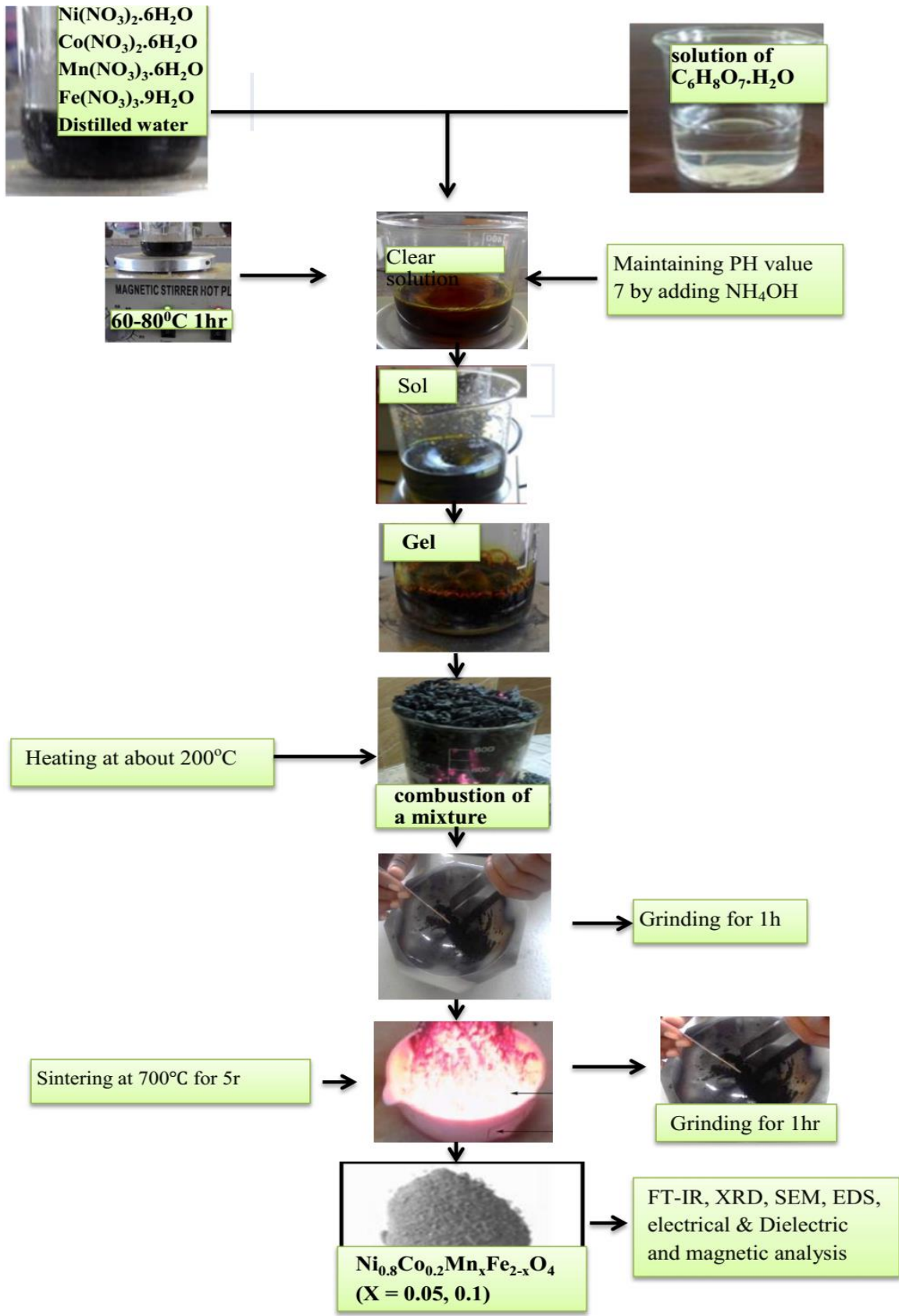


Figure3.1: Flow diagram of samples preparation

3.3.2 Pellet preparation for electrical characterization

The electrical and dielectric properties of the materials are evaluated by measuring the impedance of samples by preparing pellet. Pellet of each Nanocrystalline powder sample is prepared from the powder as an active material and polyvinyl alcohol (PVA) as a binder. First, about 2 grams of the calcined powder was initially ground in the agate mortar for about 30 minutes. Next 5 drops of polyvinyl alcohol (PVA) was added and mixed with a powder sample to bind the powder and grounded for about 10 minutes in a gate mortar well to disperse the PVA throughout the sample. Subsequently, the PVA mixed powder has been pelletized using the hydraulic press with applied pressure up to 6 tones using a die set pressure technique for 4 minutes to make 10 mm of circular disk-shaped pellets. Further, the pellet has been sintered at 900°C for 4 hrs in the air at the heating and cooling rates of 5°C/min and removed the binder. The sintered pellet was polished carefully using fine quality emery paper to make both faces flat, smooth and parallel. The thickness and the diameter of the final polished pellets were about 1.22mm and 10 mm. Further, the opposite sides of the pellets were painted with silver and heated at a temperature of 100°C for 30 minutes in order to remove the moisture. The overall flowchart for the preparation of a pellet was shown in Figure 3.2.

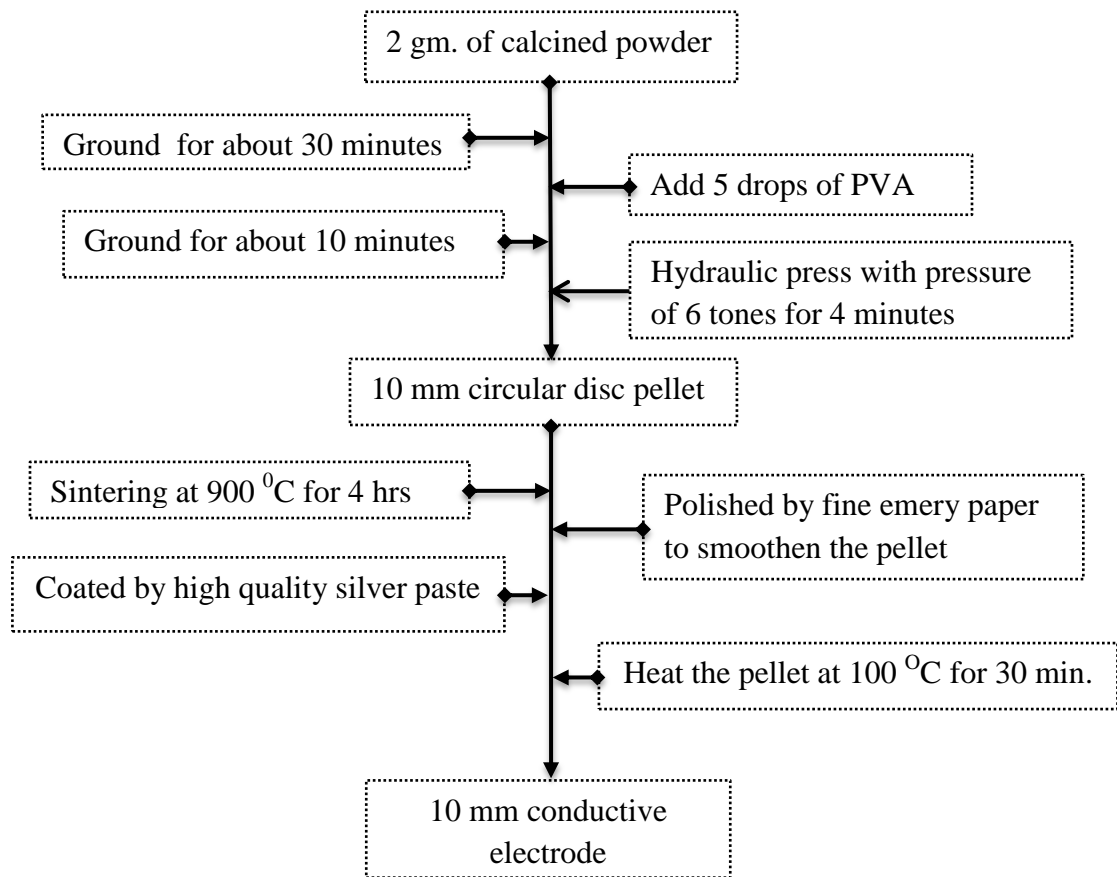


Figure 3.2 Flow chart of pellet preparation

3.4 Characterization techniques

The physical properties studies of spinel ferrite materials are investigated using various techniques by different researchers. In this study, x-ray powder diffraction, scanning electron microscopy, dispersive X-ray spectroscopy, Fourier transforms infrared spectroscopy, impedance spectroscopy and electron spin resonance spectroscopy techniques are employed to study the structure, morphology, electrical, dielectric and magnetic properties of $\text{Ni}_{0.8}\text{Co}_{0.2}\text{Mn}_x\text{Fe}_{2-x}\text{O}_4$ (where $x = 0.05, 0.1$) ferrite materials. The details of the characterization techniques are discussed briefly in the following section.

3.4.1 X-ray Powder Diffraction

X-ray diffraction aids in elucidating the arrangement and spacing of atoms in crystalline materials and used to analyze crystallite size, lattice parameter, phase identification, purity,

etc. on powder samples [47]. The wavelength of X-rays is of the order of the distance between neighboring atoms in a crystal and exhibits interference and diffraction effects. Characteristic X-rays are emitted from atomic elements when their electrons make transitions between the inner atomic energy levels. They occur when a high energy electron ionizes an inner atom and then that hole is filled by an outer shell electron. X-rays are reflected secularly from successive planes of various “hkl” families in a crystal. The diffraction maxima are obtained for directions of incidence and reflection such that reflections from adjacent planes of a family interfere constructively differing in the phase by $2\pi n$ radian (n is an integer).

The path difference for reflections between adjacent planes is given by $2d\sin\theta$ where d is the spacing between adjacent atomic planes and θ is the glancing angle between the atomic plane and the incident beam. Bragg assumed that systems of crystal planes could reflect X-rays provided the condition for constructive interference between reflections from successive atomic planes is satisfied i.e.,

$$n\lambda = 2d_{hkl}\sin\theta_{hkl} \quad (3.1)$$

where n is an integer, λ is the wavelength of an incident X-ray beam, d is the spacing between the planes in the atomic lattice, and θ is the angle between the incident ray and the scattering planes.

Here the X-ray diffraction analyses of the grown crystals have been carried out using the powder diffraction method. The finely powdered sample taken for the study consists of enormous small crystallites oriented in every possible direction. When an X-ray beam traverses the material a significant number of particles are oriented in such a way that Bragg's condition for reflection is satisfied for every possible atomic site. The detector is a scintillation counter that emits a flash of light each time an X-ray photon is absorbed. The detector is moved over a wide range of Bragg angles and the diffraction pattern is recorded as a sequence of peaks on a chart calibrated in $2\theta = 80^\circ$. The diffraction peaks so obtained are compared with X-ray powder data file published by the joint committee on powder diffraction standards (JCPDS).

Both samples synthesized in this study are characterized by powder X-ray diffraction using a Phillips XPERT-PRO diffractometer fitted with Cu $K\alpha$ radiation of wave length $\lambda = 1.54060$

Å between $2\theta = 10^\circ$ and 80° . The lattice constants, a , for the samples $\text{Ni}_{0.8}\text{Co}_{0.2}\text{Mn}_x\text{Fe}_{2-x}\text{O}_4$ ($x = 0.05$ and 0.1) are calculated by the least-square fitting method from the d -spacing and the Miller indices, hkl values using equation [37, 47].

$$a = d\sqrt{h^2 + k^2 + l^2} \text{ or } d = \frac{a}{\sqrt{h^2 + k^2 + l^2}} \quad (3.2)$$

The average crystal size, L , of the samples is estimated by using Debye-Scherrer formula [48],

$$L = \frac{0.9\lambda}{\beta \cos \theta} \quad (3.3)$$

Where λ is the wavelength of X-ray, β is the full width at half maximum (FWHM) of the diffraction peak and θ is the Bragg's angle.

The average volume, V of the sample is estimated by using Debye-Scherrer formula as,

$$V = a^3 (\text{Å})^3 \quad (3.4)$$

Where, a , for lattice constant and Å is for the unit of lattice constant, angstrom.

3.4.2 Scanning Electron Microscopy

Scanning electron microscope (SEM) is a technique in which the sample surface is scanned and analyzed when the electrons generated with an electron gun are irradiated over the sample. Electrons interact with the atoms that make up the sample producing signals which allows an image to be created by analysis of the secondary electrons and back-scattered electrons. The energy from the secondary electron is less than that of the backscattered electron which has energy close to that of the primary electron [49]. Backscattered electrons are rich in surface sensitive information, which is highly important to SEM measurement. SEM provides a variety of information about the sample, such as surface topography, composition and grain size [50].

In the present study, the microstructure and morphology of both powder samples are characterized by JEOL JSM-6610L instrument. EDS, which is coupled with SEM, technique is employed for elemental composition identification.

3.4.3 Energy dispersive X-Ray spectroscopy

Energy dispersive spectroscopy (EDS) is a technique used in identifying and quantifying the elemental composition of a sample. On irradiating the sample with electron beam, the

electrons lose energy when they interact with the sample and the lost energy will be converted into other forms such as heat, emission of secondary electrons and emission of x-rays, which can be detected by specialized detectors [51]. This change having energy proportional to the incoming x-ray is amplified and correlated to the atoms element according to its energy. However, this technique has a relatively poor energy resolution and is unable to detect lighter elements below sodium, like Hydrogen, Lithium and Helium.

3.4.4 Fourier transform infrared spectroscopy

Fourier transformed infrared (FT-IR) spectroscopy technique is used for investigating the infrared spectra in terms of absorbance or transmittance. This technique is utilized for identifying the internal structure of the molecules, and the nature of the chemical bonds in the crystal [49, 52]. It is also used to identify the structure of the unknown compound. To identify the unknown sample, the obtained absorption spectrum is compared with standard spectra in computer databases or with a spectrum of a known compound in a library.

In FT-IR, the infrared light beam containing many different frequencies is passed through a sample and the molecules in a sample will be excited into a higher vibrational state. Moreover, the absorption of infrared radiation by the sample is measured. The wavelength of light absorbed is characteristic of the chemical bonds of the molecules. The chemical bonds in a molecule can be determined by interpreting the infrared absorption spectrum and therefore the molecular components and structures can be identified.

In this study, FT-IR spectroscopy characterization technique is employed in the transmittance method with potassium Bromide (KBr) as IR window in the wave number region of 400-4,000 cm^{-1} . For the characterization of both samples, a small amount of powder sample is mixed with KBr and ground in a mortar with a pestle. The mixture is then press in a standard hydraulic press to form a transparent pellet through which the beam of the spectrometer can pass [52]. ALFA-T instrument is used for IR study of both samples.

3.4.5 Complex impedance spectroscopy

Electrochemical Impedance spectroscopy (EIS), sometimes called AC impedance spectroscopy, is a powerful characterization technique for investigating the electrical properties of materials that a lot of between parallel electrodes. It is also important to study

the correlation between complex dielectric constant, electrical susceptibility and electrical conductivity of materials. The EIS technique is based on analyzing the ac. the response of a system to a sinusoidal perturbation and subsequent calculation of the impedance as a function of the frequency of the perturbation. The technique enables an evaluation and separation of contributions to the overall electrical properties in the frequency domain due to differences in impedance of the electrode interface, migration of charge carriers across grain and grain boundaries and other phenomena. With impedance spectroscopy, a sinusoidal signal of low amplitude is applied to a sample and the complex impedance and phase shift are measured as an output. The impedance can be represented as a real (Z') and imaginary (Z'') component.

Interims of Z' and Z'' , the real dielectric constant, ε' , and imaginary parts of complex dielectric constant ε'' , are represented as [53]:

$$\varepsilon' = \frac{Z''}{\omega C (Z'^2 + Z''^2)} \quad (3.5)$$

$$\varepsilon'' = \frac{Z'}{\omega C (Z'^2 + Z''^2)} \quad \varepsilon \quad (3.6)$$

Where, ω is the radial frequency and C is the capacitance?

In this research work, the dc conductivity (σ_{dc}), the ac conductivity (σ_{ac}) and the dielectric constant (ε'), the dielectric loss (ε'') and imaginary impedance Z'' are evaluated using the relations [53, 54]:

$$\sigma_{dc} = \frac{t}{R_b A} \quad (3.7)$$

$$\sigma_{ac} = 2\pi f \varepsilon_0 \varepsilon' \tan \delta \quad (3.8)$$

$$\varepsilon' = \frac{C t}{\varepsilon_0 A} \quad (3.9)$$

$$\varepsilon'' = \varepsilon' \tan \delta \quad (3.10)$$

$$Z'' = \frac{1}{2\pi f C} \quad (3.11)$$

Where:

- t is the thickness of the pellet
- R_b is the bulk (grain) resistance
- A is the area of the pellet
- ϵ_0 is the permittivity of the free space
- $\tan\delta$ is dielectric loss tangent
- C is the capacitance
- f is the frequency

3.4.6 Electron spins resonance spectroscopy

The magnetic property of atoms or molecules is originated from their electrons and nucleus. This property can be investigated by using electron spin resonance (ESR) and nuclear magnetic resonance (NMR) spectroscopies. ESR requires microwave frequency radiation (GHz), while NMR is observed at lower radio *frequencies* (MHz). ESR spectroscopy, which is also called electron paramagnetic resonance (EPR) spectroscopy, is a useful tool for studying the magnetic properties of materials. Measurements of the magnetic moment provide information about the local magnetic properties, the nature of spin-spin interactions, the distribution of internal field and spin-lattice correlations. ESR measurements are usually made by scanning the magnetic induction (B) at constant frequency of microwave through the range of interest. The position of the ESR line depends on the ratio of B to the frequency f and the effective gyromagnetic factor (g). From the width and shape of the resonant line, we can obtain detailed information on magnetic state. In this study, the ESR spectra of $\text{Ni}_{0.8}\text{Co}_{0.2}\text{Mn}_x\text{Fe}_{2-x}\text{O}_4$ (where $x = 0.05, 0.1$) samples are conducted at 650mT at room temperature using the instrument Magnetometer.

CHAPTER FOUR

RESULT AND DISCUSSION

4.1 XRD analysis

In order to confirm the phase formation of $\text{Ni}_{0.8}\text{Co}_{0.2}\text{Mn}_x\text{Fe}_{2-x}\text{O}_4$ with compositions 0.05 and 0.1 nanoparticles, XRD study is carried out for two prepared samples. Figure 4.1 shows the XRD patterns of $\text{Ni}_{0.8}\text{Co}_{0.2}\text{Mn}_{0.05}\text{Fe}_{1.95}\text{O}_4$ and $\text{Ni}_{0.8}\text{Co}_{0.2}\text{Mn}_{0.1}\text{Fe}_{1.9}\text{O}_4$ ferrites synthesized by sol-gel auto combustion synthesis method. From the figure it can be seen that all peaks are very sharp and well-defined, indicating the formation of highly crystalline powders and the complete formation of the Ni-Co-Mn ferrite phase. For XRD patterns of $\text{Ni}_{0.8}\text{Co}_{0.2}\text{Mn}_{0.05}\text{Fe}_{1.95}\text{O}_4$ shown in figure 4.1 (a), the diffraction peaks are formed at 2θ angles of 17.61° , 29.18° , 34.62° , 36.3° , 42.26° , 52.63° , 56.21° , 61.8° , 70.37° , 73.2° & 74.38° . Their corresponding diffraction angles are marked by (111), (220), (311), (222), (400), (422), (511), (440), (620), (533) and (622), respectively. No other phases or extra peaks are identified, which indicates the formation of single phase spinel with cubic structure of MgAl_2O_4 .

For the case $\text{Ni}_{0.8}\text{Co}_{0.2}\text{Mn}_{0.1}\text{Fe}_{1.9}\text{O}_4$ powder sample, the diffraction peaks are formed at 2θ angles of 17.51° , 29.03° , 34.47° , 36.04° , 42.11° , 52.47° , 56.05° , 61.48° , 70.14° , 73.07° & 74.22° . Their corresponding diffraction angles are marked by (111), (220), (311), (222), (400), (422), (511), (440), (620), (533) and (622), respectively. No other phases or extra peaks are also identified, which indicates the formation of single phase spinel with cubic structure of MgAl_2O_4 . In comparison with $\text{Ni}_{0.8}\text{Co}_{0.2}\text{Mn}_{0.05}\text{Fe}_{1.95}\text{O}_4$ and $\text{Ni}_{0.8}\text{Co}_{0.2}\text{Mn}_{0.1}\text{Fe}_{1.9}\text{O}_4$, the diffraction peaks of $\text{Ni}_{0.8}\text{Co}_{0.2}\text{Mn}_{0.05}\text{Fe}_{1.95}\text{O}_4$ are slightly shifted towards higher diffraction angles (or lower d value), suggesting a decrease in cell volume or lattice parameter.

In order to study the effect of Mn^{3+} substitution on the lattice parameters, unit cell volume and crystal size of $\text{Ni}_{0.8}\text{Co}_{0.2}\text{Mn}_{0.05}\text{Fe}_{1.95}\text{O}_4$ and $\text{Ni}_{0.8}\text{Co}_{0.2}\text{Mn}_{0.1}\text{Fe}_{1.9}\text{O}_4$ ferrites, their lattice parameters are calculated by using equation (3.2), the average crystal sizes by (3.3) and the unit cell volumes by equation (3.4). The obtained results are shown in Table 4.1. From the

table it can be seen that the lattice parameter, unite cell volume and crystal size of $\text{Ni}_{0.8}\text{Co}_{0.2}\text{Mn}_{0.05}\text{Fe}_{1.95}\text{O}_4$ are lower than $\text{Ni}_{0.8}\text{Co}_{0.2}\text{Mn}_{0.1}\text{Fe}_{1.9}\text{O}_4$. This decrease is attributable to the smaller ionic radius of Fe^{3+} (0.64\AA) than Mn^{3+} (0.65\AA). In addition to this, the average crystallite size calculated using Debye–Scherer equation confirms the Nano crystalline nature of the samples.

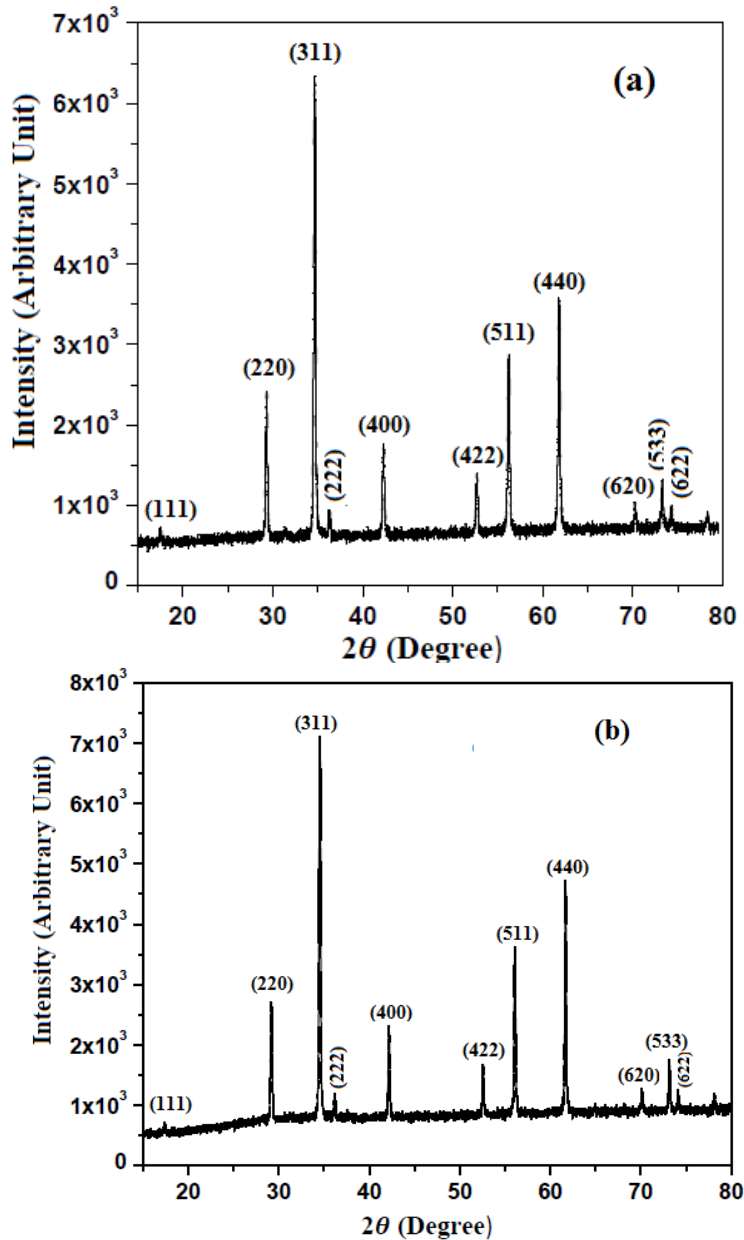


Figure 4.1 X-ray diffraction patterns of (a) $\text{Ni}_{0.8}\text{Co}_{0.2}\text{Mn}_{0.05}\text{Fe}_{1.95}\text{O}_4$ and (b) $\text{Ni}_{0.8}\text{Co}_{0.2}\text{Mn}_{0.1}\text{Fe}_{1.9}\text{O}_4$ ferrites.

Table 4.1 Lattice constant, 2θ , intensity, d-spacing, cell volume and crystal size of Synthesized samples

Samples	2θ value for (400) (degree)	Intensity I for (400)	d-spacing for (400) (Å)	Lattice Constant (Å)	Unite Cell Volume (Å) ³	Crystal Size from (311) (nm)
Ni _{0.8} Co _{0.2} Mn _{0.05} Fe _{1.95} O ₄	42.26	1762.323	2.13452	8.538	622.4	58.23
Ni _{0.8} Co _{0.2} Mn _{0.1} Fe _{1.9} O ₄	42.11	2319.83	2.14031	8.561	627.44	59.14

4.2 SEM and EDS Analysis

As discussed in chapter 3, scanning electron microscopy is a powerful technique on the investigation of different materials. It gives the information on the morphology, shape and size of particles making up the material, direct relation between the structures and materials properties. Figure 4.2 shows the SEM images of Ni_{0.8}Co_{0.2}Mn_{0.05}Fe_{1.95}O₄ and Ni_{0.8}Co_{0.2}Mn_{0.1}Fe_{1.9}O₄ ferrites in the form of powder. From the SEM images, it is seen that in both samples the particles have slightly porous structure and some of them are in agglomerated. From the grain size point of view, morphological changes are clearly seen as a result of Mn³⁺ substitution and it is observed that the grain sizes are increased with increasing Mn³⁺ content in the prepared samples. The obtained results are consistent with the calculated lattice parameters and crystal sizes from XRD patterns. It is also observed that agglomeration as well as size of the pores of the compound is increased with the change in the composition of Mn³⁺ in the sample from $x = 0.05$ to $x = 0.1$.

The Characteristic information obtained from the SEM images finally concluded as Small pores were seen between neighboring particles, the particle was distributed in different sizes, agglomerated particles were observed, and the grain sizes and the agglomeration of particles increased with increasing the Mn content.

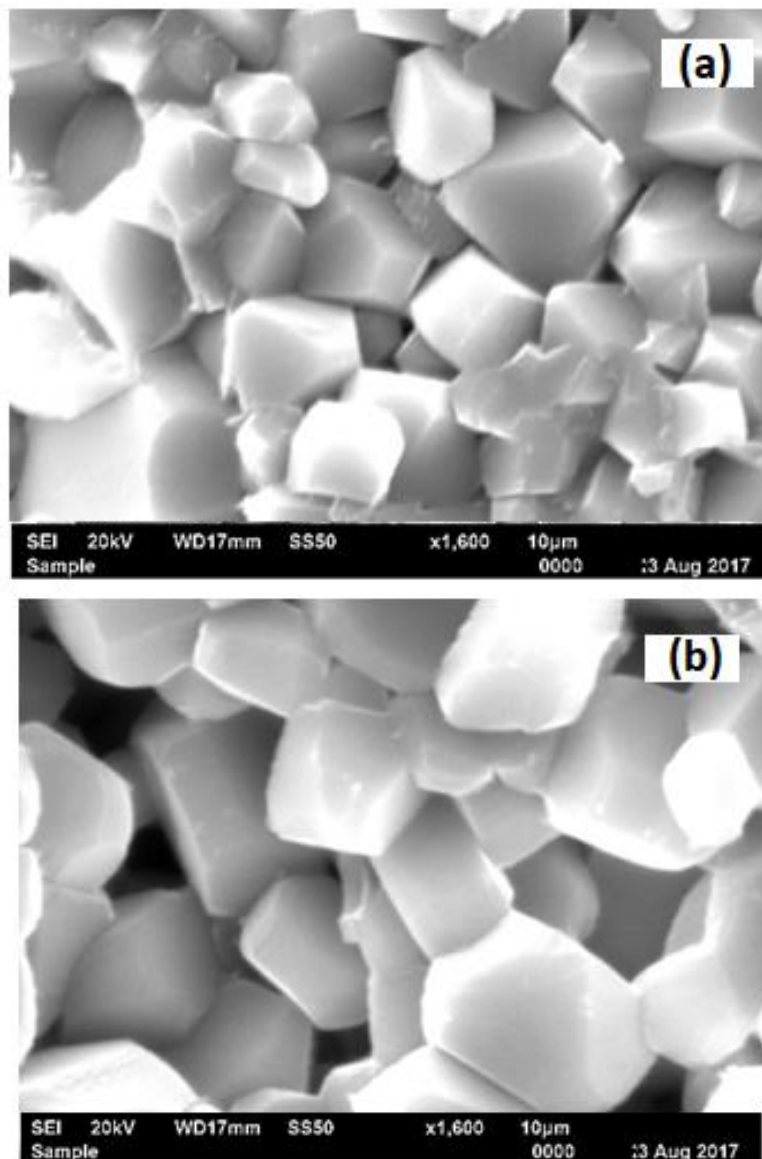


Figure 4.2 Scanning electron micrographs of (a) $\text{Ni}_{0.8}\text{Co}_{0.2}\text{Mn}_{0.05}\text{Fe}_{1.95}\text{O}_4$ and
b) $\text{Ni}_{0.8}\text{Co}_{0.2}\text{Mn}_{0.1}\text{Fe}_{1.9}\text{O}_4$ ferrites.

The elemental analysis of $\text{Ni}_{0.8}\text{Co}_{0.2}\text{Mn}_{0.05}\text{Fe}_{1.95}\text{O}_4$ and $\text{Ni}_{0.8}\text{Co}_{0.2}\text{Mn}_{0.1}\text{Fe}_{1.9}\text{O}_4$ ferrite samples with different compositions is analyzed by Energy Dispersive Spectrometer (EDS). The EDS spectra for both ferrites are shown in the Figure 4.3 which indicates the elemental and atomic composition in the sample. It can be observed that both compounds show the presence of Ni, Co, Mn, Fe and O. As compared all these elements, the elemental levels of Fe and O are significantly higher than other elements. No other elements are detected in the investigated ferrite, which indicates the high purity of the synthesized products. This is consistent with the result obtained in the XRD patterns.

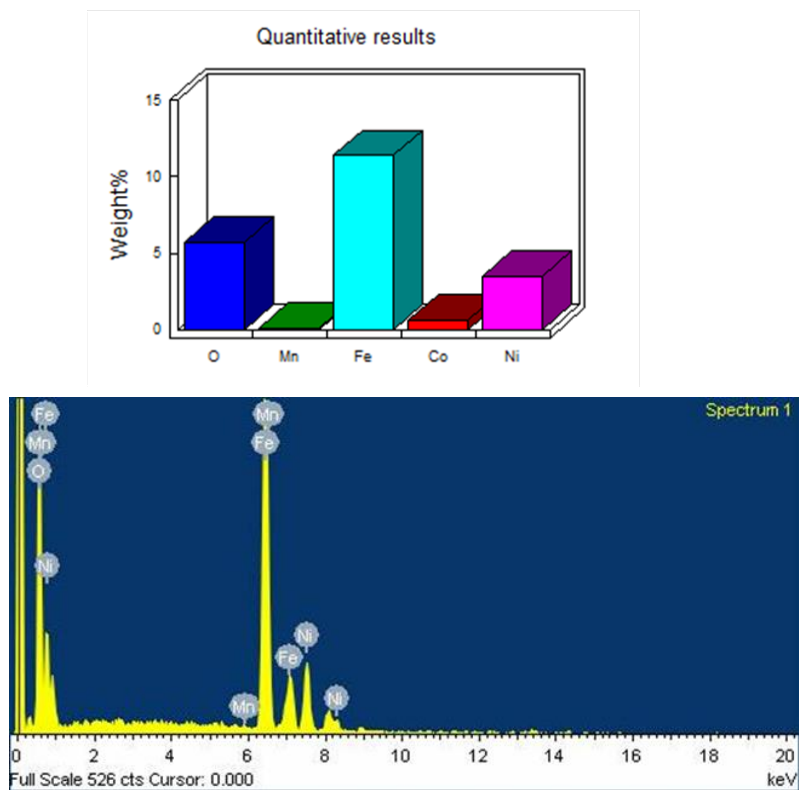


Figure 4.3: (a) EDX spectra and elemental analysis for $\text{Ni}_{0.8}\text{Co}_{0.2}\text{Mn}_{0.05}\text{Fe}_{1.95}\text{O}_4$ ferrite material.

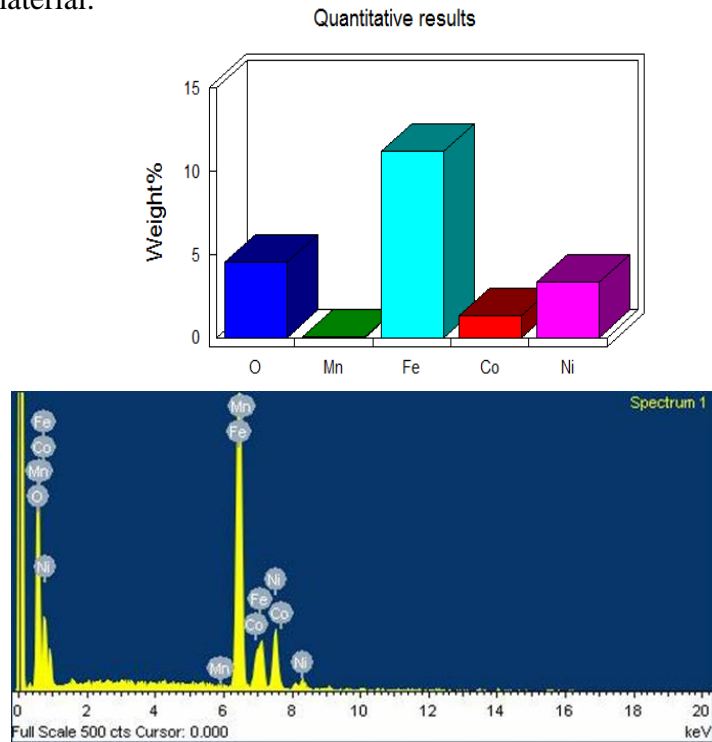


Figure 4.3: (b) EDX spectra and elemental analysis for $\text{Ni}_{0.8}\text{Co}_{0.2}\text{Mn}_{0.1}\text{Fe}_{1.9}\text{O}_4$ ferrite Material.

4.3 FT-IR Analysis

The FT-IR spectra for $\text{Ni}_{0.8}\text{Co}_{0.2}\text{Mn}_{0.05}\text{Fe}_{1.95}\text{O}_4$ and $\text{Ni}_{0.8}\text{Co}_{0.2}\text{Mn}_{0.1}\text{Fe}_{1.9}\text{O}_4$ compounds in the form of powder synthesized by sol-gel auto combustion method at a temperature of $700\text{ }^\circ\text{C}$ in the range of $400\text{--}4000\text{ cm}^{-1}$ analyzed by FT-IR at room temperature are shown in Figure 4.4 (a) and (b). It is known that in all spinel ferrites, two main broad metal oxygen bands are seen in the FT-IR spectra [49], one is around 600 cm^{-1} and the other is around 400 cm^{-1} . As shown in the figure, two strong bands are appeared at 591.2 cm^{-1} and 588.3 cm^{-1} from $\text{Ni}_{0.8}\text{Co}_{0.2}\text{Mn}_{0.05}\text{Fe}_{1.95}\text{O}_4$ and $\text{Ni}_{0.8}\text{Co}_{0.2}\text{Mn}_{0.1}\text{Fe}_{1.9}\text{O}_4$ ferrites, respectively. However, the next expected bands which are assumed to be found around 400 cm^{-1} are not observed.

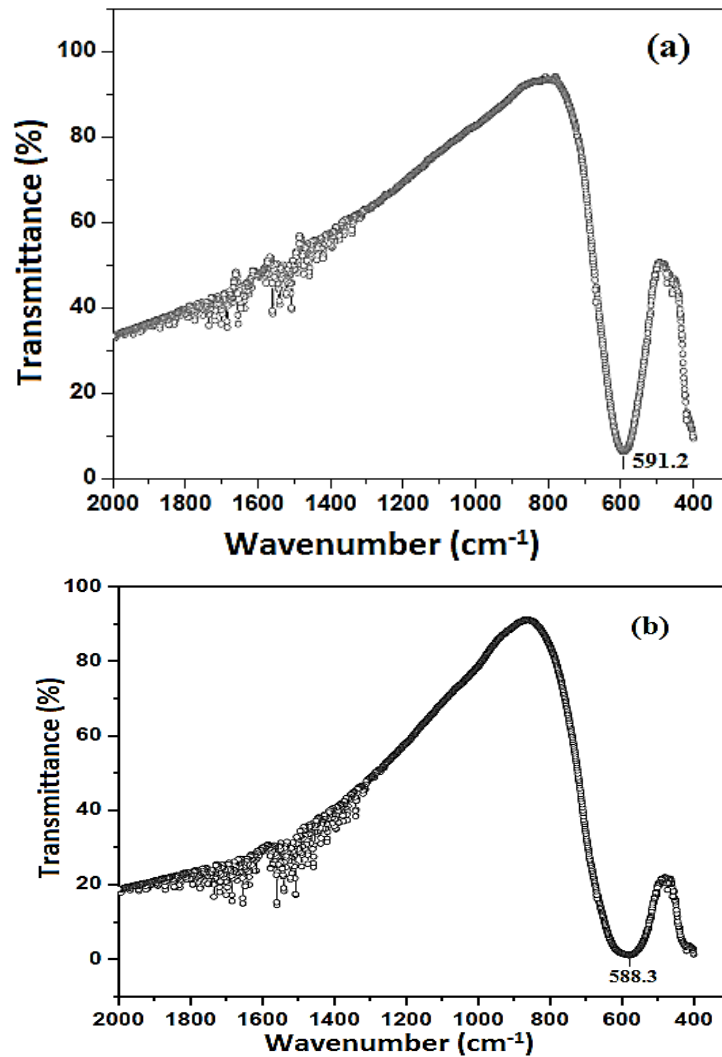


Figure 4.4: FT-IR spectra of (a) $\text{Ni}_{0.8}\text{Co}_{0.2}\text{Mn}_{0.05}\text{Fe}_{1.95}\text{O}_4$ and (b) $\text{Ni}_{0.8}\text{Co}_{0.2}\text{Mn}_{0.1}\text{Fe}_{1.9}\text{O}_4$ ferrites.

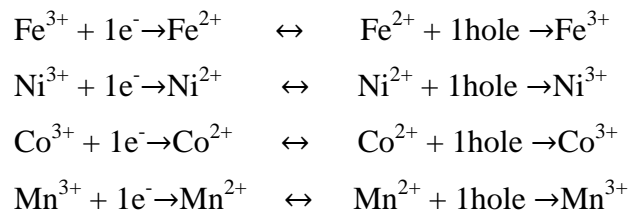
The obtained bands appearing at the higher wavenumber are assigned to the tetrahedral A site, which may be due to the stretching vibration of Mn-Fe-O. On the other hand, due to the formation of $\text{Ni}_{0.8}\text{Co}_{0.2}\text{Mn}_{0.1}\text{Fe}_{1.9}\text{O}_4$ material, the peak is shifted slightly towards lower wavenumber, i.e. 588.3 cm^{-1} (Figure 4.3 b), which is consistent with the assumption deduced from XRD results. This may be due to the longer bond length of the tetrahedral site of $\text{Ni}_{0.8}\text{Co}_{0.2}\text{Mn}_{0.1}\text{Fe}_{1.9}\text{O}_4$ than that of the tetrahedral site of $\text{Ni}_{0.8}\text{Co}_{0.2}\text{Mn}_{0.05}\text{Fe}_{1.95}\text{O}_4$. It is also in good agreement with the larger lattice parameter; unit cell volume and crystal size of $\text{Ni}_{0.8}\text{Co}_{0.2}\text{Mn}_{0.1}\text{Fe}_{1.9}\text{O}_4$ sample calculated from the obtained XRD pattern.

4.4 Electrical and dielectric properties studies

4.4.1 Variation of conductivity with frequency

To study the variation of ac conductivity with frequency, the ac conductivity is calculated using equations (3.8). Figure 4.5 (a) and (b) shows the variation of conductivity with frequency at room temperature for $\text{Ni}_{0.8}\text{Co}_{0.2}\text{Mn}_x\text{Fe}_{2-x}\text{O}_4$ (where $x = 0.05, 0.1$) ferrite electrodes. As can be observed, two different regions are clearly obtained in both samples. The first one is frequency independent plateau region and the second one is the frequency dependent region, which corresponds to the frequency dependent conductivity region. A significant change in conductivity is observed at higher frequencies. The frequency independent plateau at low frequencies indicates the contribution of the dc conductivity, which is due to the electrode polarization effect [4, 55]. It is clearly observed that the dc conductivity continues until hopping of charges occurs and this variation remains the same for both samples with different manganese concentrations. Further, both samples exhibit increases in ac conductivity with the increase in frequency which may be ascribed as the normal behavior of ferrites.

In addition to the above information, a significant change occurred in conductivity shown by frequency increase is due to the release of excess ions from both tetrahedral and octahedral sites. Here under the overall collective of hopping of charges in this dc and ac study [55] as:



This confirms the semiconducting behavior for conductivity, i.e. due to this existence of M^{3+} ions the materials act as n-type behavior and due to that of M^{2+} ions they act as p-type behavior.

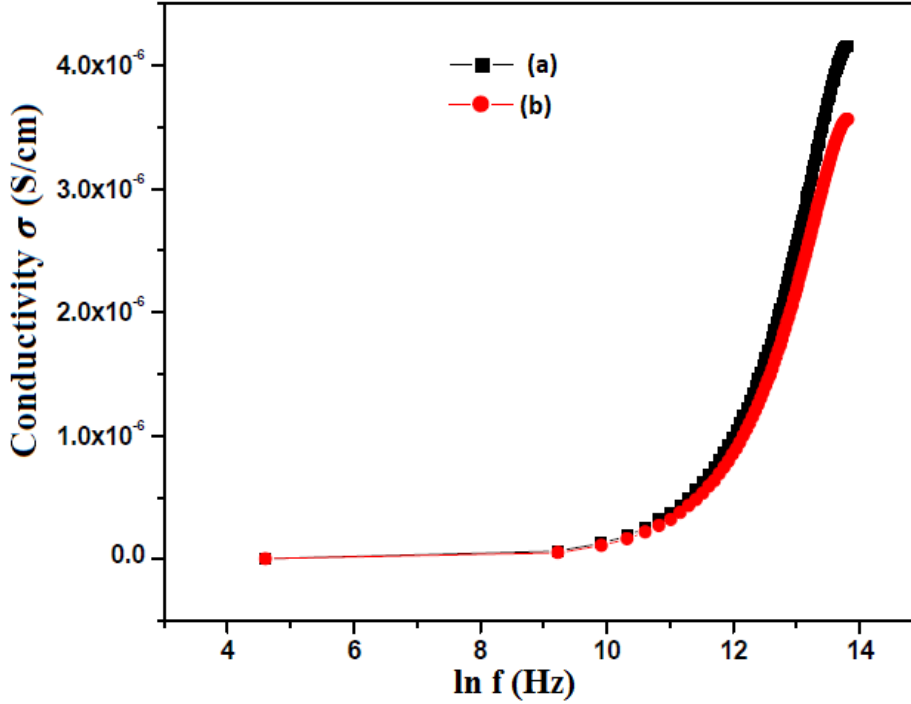


Figure 4.5 Variation of conductivity with frequency of (a) $Ni_{0.8}Co_{0.2}Mn_{0.05}Fe_{1.95}O_4$ and (b) $Ni_{0.8}Co_{0.2}Mn_{0.1}Fe_{1.9}O_4$ ferrites.

4.4.2 Variation of dielectric constant with frequency

To study the variation of dielectric constant ϵ' with frequency, ϵ' is calculated using equation (3.9). Figure 4.6 shows the variation of dielectric constant with a frequency of $Ni_{0.8}Co_{0.2}Mn_{0.05}Fe_{1.95}O_4$ and $Ni_{0.8}Co_{0.2}Mn_{0.1}Fe_{1.9}O_4$ ferrites synthesized by sol-gel auto-combustion method. It is found that the value of the dielectric constant is decreased with increasing frequency for both the samples, which can be considered as a normal dielectric behavior of ferrites. The variation of dielectric constant can be related to the collective behavior of the electric charge carrier's electrons and holes. This has been explained on the basis of the Rezlescu model reported in [56]. According to this model, the electric charges exchanging between $Fe^{2+} \leftrightarrow Fe^{3+}$, $Co^{2+} \leftrightarrow Co^{3+}$, $Ni^{2+} \leftrightarrow Ni^{2+}$ and $Mn^{3+} \leftrightarrow Mn^{2+}$ are responsible for electric conduction and dielectric polarization in $Ni_{0.8}Co_{0.2}Mn_xFe_{2-x}O_4$ (where

x = 0.05, 0.1) electrodes. During this process, localized electric charges accumulation takes place.

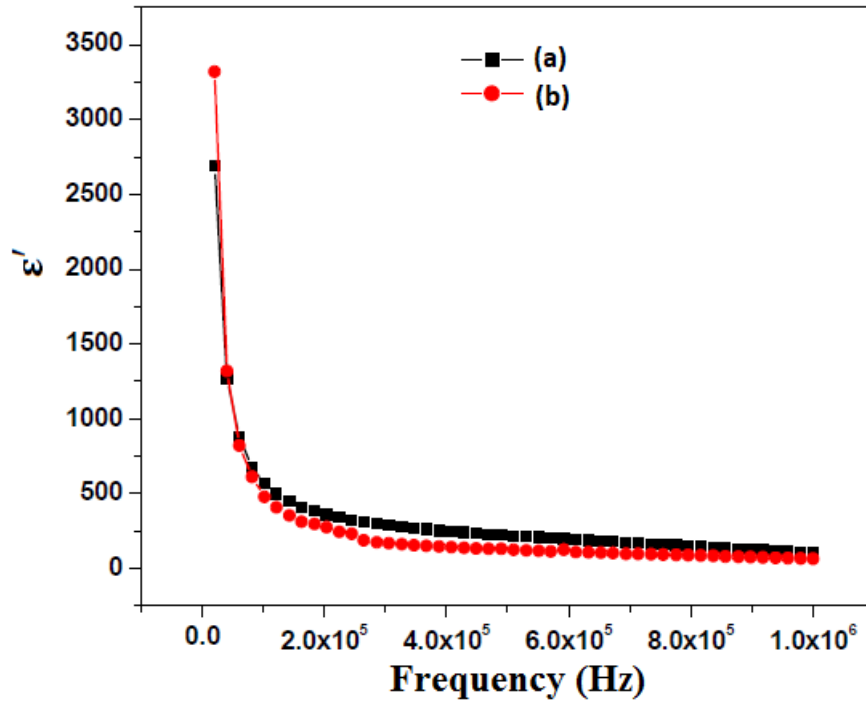


Figure 4.6 Variation of dielectric constant ϵ' with frequency of (a) $\text{Ni}_{0.8}\text{Co}_{0.2}\text{Mn}_{0.05}\text{Fe}_{1.95}\text{O}_4$ & (b) $\text{Ni}_{0.8}\text{Co}_{0.2}\text{Mn}_{0.1}\text{Fe}_{1.9}\text{O}_4$ ferrites.

4.5 Magnetic properties study

The magnetic properties of ferrites mainly depend on their chemical composition, crystal structure, cation distribution and microstructure. From the measured hysteresis loops, we can determine the magnetization saturation (M_s), coercivity (H_c) and remnant magnetization (M_r). The room temperature magnetic properties of the $\text{Ni}_{0.8}\text{Co}_{0.2}\text{Mn}_{0.05}\text{Fe}_{1.95}\text{O}_4$ and $\text{Ni}_{0.8}\text{Co}_{0.2}\text{Mn}_{0.1}\text{Fe}_{1.9}\text{O}_4$ nanoferrite which are characterizing using ESR technique with an applied field of $-15,000 \text{ Oe} \leq H \leq 15,000 \text{ Oe}$ are shown in Figure 4.7 (a) and (b).

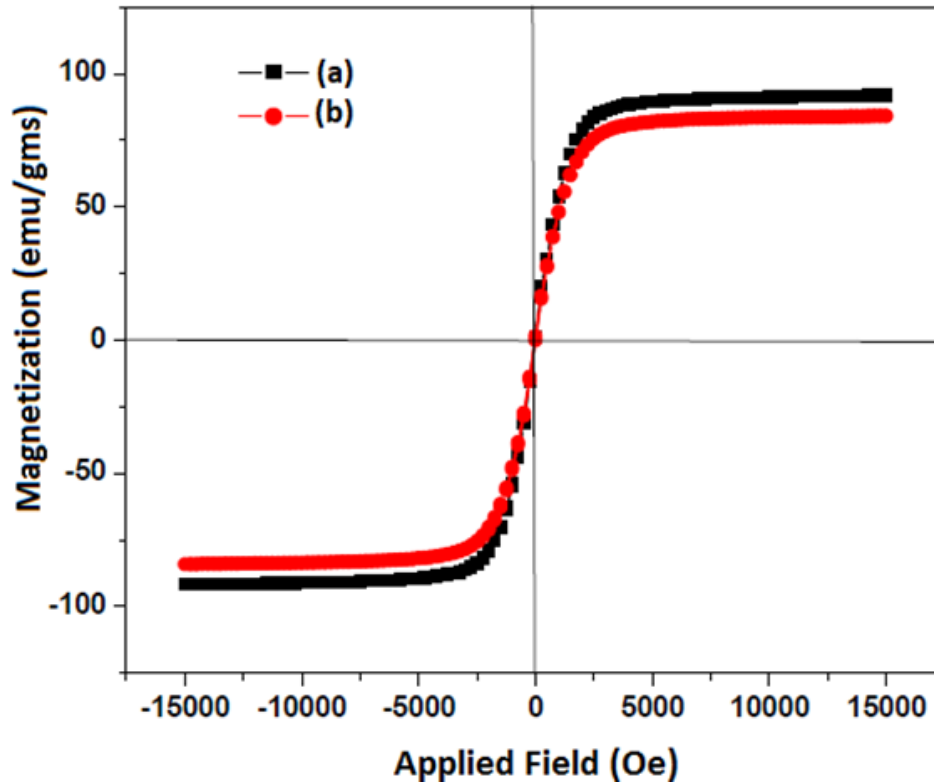


Figure 4.7 Magnetic hysteresis loops for (a) $\text{Ni}_{0.8}\text{Co}_{0.2}\text{Mn}_{0.05}\text{Fe}_{1.95}\text{O}_4$ and (b) $\text{Ni}_{0.8}\text{Co}_{0.2}\text{Mn}_{0.1}\text{Fe}_{1.9}\text{O}_4$ nanoferrite at room temperature.

It can be observed from the Figure 4.7; both the nanomaterials show soft magnetization behavior at room temperature. Thus, the magnetization curve of both samples shows weak ferromagnetic behavior, with slender S shaped hysteresis. It is also found that the specific saturation magnetization (M_s) of $\text{Ni}_{0.8}\text{Co}_{0.2}\text{Mn}_{0.05}\text{Fe}_{1.95}\text{O}_4$ nanoferrite sample is nearly 91 emu/gms. For $\text{Ni}_{0.8}\text{Co}_{0.2}\text{Mn}_{0.1}\text{Fe}_{1.9}\text{O}_4$ nanoferrite, the saturation magnetization is found to be 83.58 emu/gms. However, remnant magnetization, coercivity field are not identified from the figure, indicating the super paramagnetic nature of both nanoferrites. From this, it can be suggested that the cation distribution in both nanoferrite materials is partly inverted and exhibits anomaly in its magnetization, which can exhibit super paramagnetic and weak ferromagnetic characteristic of these nanomaterials.

The variation of magnetic properties of both Nanofibers can be understood in terms of cation distribution and exchange interactions between spinel lattices. As compared the magnetic properties of both samples, $\text{Ni}_{0.8}\text{Co}_{0.2}\text{Mn}_{0.05}\text{Fe}_{1.95}\text{O}_4$ exhibits larger values of magnetization than $\text{Ni}_{0.8}\text{Co}_{0.2}\text{Mn}_{0.1}\text{Fe}_{1.9}\text{O}_4$ nanoferrite. The smaller in magnetization for

$\text{Ni}_{0.8}\text{Co}_{0.2}\text{Mn}_{0.1}\text{Fe}_{1.9}\text{O}_4$ may be attributed to the fact that, larger amount of Mn^{3+} ions substituted for Fe^{3+} decrease the content of Fe^{3+} ions. This leads to a decrease of magnetic moment. So, the net magnetization decreases, which is consistent with the decrease of saturation magnetization.

CHAPTER FIVE

CONCLUSION AND RECOMMENDATION

5.1 Conclusion

In this study, $\text{Ni}_{0.8}\text{Co}_{0.2}\text{Mn}_x\text{Fe}_{2-x}\text{O}_4$ (where $x = 0.05$ & 0.1) nanocrystalline powder materials are successfully synthesized by sol-gel auto-combustion synthesis method using $\text{Ni}(\text{NO}_3)_2 \cdot 6\text{H}_2\text{O}$, $\text{Co}(\text{NO}_3)_2 \cdot 6\text{H}_2\text{O}$, $\text{Mn}(\text{NO}_3)_3 \cdot 6\text{H}_2\text{O}$ and $\text{Fe}(\text{NO}_3)_3 \cdot 9\text{H}_2\text{O}$ raw materials. Citric acid is used as chelating agent during the preparation process. The synthesized powder materials are characterized by XRD, SEM, EDS, FT-IR spectroscopy, ESR spectroscopy and impedance analyzer. From this investigation, the following conclusions are drawn:

XRD, FT-IR spectroscopy and EDS confirm the phase purity of the synthesized ferrites. XRD analysis shows all peaks of the synthesized nanoferrites are very sharp and well-defined, indicating the highly crystallinity of these materials. It also confirms the formation of cubic spinel structure with space group $\text{Fd}\bar{3}\text{m}$. It also shows the lattice parameter, unit cell volume and crystal size of both synthesized ferrites are influenced by the amount of the Mn substitution. An increase in the Mn content from $x = 0.05$ to 0.1 into $\text{Ni}_{0.8}\text{Co}_{0.2}\text{Mn}_x\text{Fe}_{2-x}\text{O}_4$ leads to an increase in lattice parameter, unit cell volume as well as crystal size.

SEM images show the variation of grains with the variation of the amount of substitution of Mn for Fe in the synthesized ferrites. It also confirms that both synthesized ferrite materials have slightly porous structure. EDS patterns confirm the compositional formation of the synthesized samples, i.e., both synthesized ferrites show the presence of Ni, Co, Mn, Fe and O elements.

FT-IR spectra analysis reveals the appearance of strong absorption bands at 591.2 and 588.3 cm^{-1} from $\text{Ni}_{0.8}\text{Co}_{0.2}\text{Mn}_{0.05}\text{Fe}_{1.95}\text{O}_4$ and $\text{Ni}_{0.8}\text{Co}_{0.2}\text{Mn}_{0.1}\text{Fe}_{1.9}\text{O}_4$ ferrites, respectively. These bands are responsible for the formation of cubic spinel structure.

From the frequency dependent plot of dielectric constant, it is observed that for each sample decreases sharply as the frequency increases and becoming almost constant at higher frequencies. Similarly, from the plots of ac conductivity, the frequency dependent and non-frequency-dependent regions are identified.

The magnetic property study confirms the soft magnetization behavior of the synthesized nanoferrite materials at room temperature. It is also found that $\text{Ni}_{0.8}\text{Co}_{0.2}\text{Mn}_{0.05}\text{Fe}_{1.95}\text{O}_4$ and $\text{Ni}_{0.8}\text{Co}_{0.2}\text{Mn}_{0.1}\text{Fe}_{1.9}\text{O}_4$ nanoferrites exhibit 91 emu/gms and 83.5.8 emu/gms specific saturation magnetization (Ms), respectively.

5.2 Recommendation

From the past historical development in the nanotechnology, ferrites- ceramic ferromagnetic materials have been considered as highly economically useful materials for many purposes. Nowadays, due to their remarkable commercial significance, the quality of commercial ferrites has been improved by doping one into another through accumulated scientific knowledge and advanced technology. In this study, manganese substituted iron deficiency nickel ferrite having chemical composition $\text{Ni}_{0.8}\text{Co}_{0.2}\text{Mn}_x\text{Fe}_{2-x}\text{O}_4$ where $x = 0.05$ & 0.1 , are prepared by the sol-gel auto combustion method. We tried to study the structure, morphology, chemical compositions, and electrical, dielectric and magnetic properties of the synthesized materials.

However, the electrical, magnetic and dielectric properties of the materials at different temperature ranges are not included in this study. Therefore, in our further studies could have to consider them for additional understanding and giving concrete conclusion on the ferrite materials. Additionally, systematic investigation of the structure, morphology, electrical, magnetic as well as dielectric properties of these materials at different compositions, i.e., $x = 0.15, 0.2, 0.3$, etc. at room and higher temperatures to be considered in the future work.

The thermogravimetric analysis (TGA) and differential thermal analysis (DTA) are important characterization techniques to study weight loss or gain of a phase due to gas absorption or release thermal degradation of nitrate-citrate solution by degradation, decomposition of citrate to carbonate and formation of ferrite are not included in this thesis work is considered to be included in the future study.

REFERENCES

- [1] Berchmans, L.J., Senguttuvan, G., & Umapathy, G. (2014). Investigation on combustion synthesis of nanocrystalline nickel ferrite using sodium azide as a potential fuel. *International Journal of Chemical Technology Research*, 7, 131-137.
- [2] Jaswal, L., & Singh, B. (2014). Ferrite materials. *Journal of integrated Science technology*, 2(2), 3.
- [3] Aswathy E. K., Babu, A., Binu, K. T., Kurian, M., Thankachan, S., NAIR, S. D., & Thomas, A. (2015). Structural, magnetic, and acidic properties of cobalt ferrite nanoparticles synthesized by wet chemical methods. *Journal of Advanced Ceramics*, 4(3), 199–205.
- [4] Kambale, R. C., Kolekar, Y. D., Rao, A. V., & Shaikh, P.A. (2010). Studies on structural and electrical properties of $\text{Co}_{1-x}\text{Ni}_x\text{Fe}_{1.9}\text{Mn}_{0.1}\text{O}_4$ ferrite. *Journal of Alloys & Compounds*, 492, 590–596.
- [5] Costa, L. J. D., de Freitas, M. R., de Gouveia, de Oliveira, A. J. A., & Kiminami, R. H. G. A. G. L. (2016). Microwave-Assisted Combustion Synthesis & Characterization of Nanocrystalline Nickel-doped Cobalt Ferrites. *Journal of material research*, 1-6.
- [6] Kesavamoorthi, R., Raja, C. R., Sanyal, V., & Vigneshwaran, A. N. (2016). Synthesis and characterization of nickel ferrite nanoparticles by sol-gel auto combustion method. *Journal of Chemical & Pharmaceutical Sciences*, 9, 160-161.
- [7] Molakeri, S., Kumar, A., & Kalyane, S. (2016). *Synthesis and Characterization of Nano Crystalline Nickel Ferrite*. University of Bhalki, Karnataka, India.
- [8] Elhaleem. S. M. S. A. (2013). Effect of Radiation and Doping on the Structure and Physical Properties of Some Oxide Materials. MSc. Dissertation. University of Helwan.
- [9] Durrani, K. S., Iqbal, Y., Hussain, Z. S., Javed, M., Khan, A., Khan, R. A., & Majeed, A. (2017). Influence of preparation method on structural, optical and magnetic properties of nickel ferrite nanoparticles. *Journal of Materials Science*. 35(1), 58-65
- [10] Majhi, S. (2013). *Dielectric and Magnetic behavior of Substituted Strontium M Hexagonal Ferrite*. BSc. Dissertation. National institute of technology Rourkela, India.

- [11] Krishna, R. K., Ravinder, D., Kumar, V. K., & Abraham L. Ch. (2012). Synthesis, XRD & SEM Studies of Zinc Substitution in Nickel Ferrites by Citrate Gel Technique. *World Journal of Condensed Matter Physics*, 2, 153-159.
- [12] Islam, S., Mahmud, A., & Nahar, S. S. (2016). Effect of Tn (Tin) alloying on Ni-Zn ferrites characteristics. *International Journal of Advances in Materials Science and Engineering*, 5(1), 1-10.
- [13] Bhosale, C. H., Bilur, V. A., Harale, N. S., Kambale, R.C., Kolekar, Y. D., Rajpure, K.Y., & Shaikh, P.A. (2010). Structural and magnetic properties of $\text{Co}_{1-x}\text{Mn}_x\text{Fe}_2\text{O}_4$ spinel ferrites synthesized by combustion route. *Journal of Alloys and Compounds*, 490, 568–571.
- [14] Gafur, M. A., Kabir, H., Rashid, M., & Rahaman, M. (2015). Investigation of the Structural, Dielectric and Electrical properties of Zn-substituted Li-Ni ferrite. *Journal of applied Physics*, 7(1), 76-83
- [15] Naseri, M. G., & Saion, E. B. (2012). Crystallization in Spinel Ferrite Nanoparticles. *Journal of Intech open science open mind*, 66(380), 350-362.
- [16] Zaka, U., Shahid, A., & Shahzad, N. (2013). Influence of Pb doping on structural, electrical and magnetic properties of Sr-Hexaferrites. *Journal of Alloys and Compounds*. 555, 263–267
- [17] Ahmed, F., Akhter, S., Bashar, M. S., Hossain, A., Hossain, T., Rahaman, MD. M., Rahman, M. M., Pervin, S., Sheak, MD. S., & Uddin, N. (2012). Composition, temperature and frequency dependent magnetic, dielectric and electrical properties of magnesium-zinc ferrites. *Journal of Bangladesh Academy of Sciences*, 36(2), 199-212.
- [18] Atiq, Naseem, Shahid, Shahzad, Ullah, & Zaka (2013). Influence of Pb doping on structural, electrical and magnetic properties of Sr-Hexaferrites. *Journal of Alloys and Compounds*, 555, 263–267.
- [19] Sathishkumar, G., Sivakumar, K. & Venkataraju, C. (2010). Effect of cation distribution on the structural and magnetic properties of nickel substituted Nano sized Mn-Zn ferrites prepared by co-precipitation method. *Journal of Magnetism and Magnetic Materials*, 322(2), 230-233.

- [20] Borhan, A. I. (2013). *Synthesis and characterization of spinel oxide compounds AB_2O_4* . PhD Dissertation. University of Alexandru Ioan Cuza, Iasi.
- [21] Szalay, B. (2012). *Iron oxide nanoparticles and their toxicological effects: in vivo and in vitro studies*. PhD Dissertation. University of Szeged, Szeged.
- [22] Kamaruddin, A. M., Leng, L. P., Naseri, G. M., Saion, E., & Shaari, H. A. (2013). Synthesis and Characterization of Ni-Zn Ferrite Nanoparticles ($Ni_{0.25}Zn_{0.75}Fe_2O_4$) by thermal treatment method. *Journal of advances in Nanoparticles*, 2, 378-383.
- [23] Panda R. K. (2015). *Studies on Electric and Magnetic Properties of Cobalt Ferrite and its Modified Systems*. PhD Dissertation. National Institute of Technology, Rourkela, India
- [24] Duc Vu Quyen, N., Minh Hai, H. V., Minh Ngoc, T., Tuyen, T. N., & Xuan Tin, D. (2015). A Study on the synthesis of $MgAl_2O_4$ Spinel by starch assisted sol-gel process. *Journal of ceramic materials*, 53 (4), 433-440
- [25] Agrawal, H. M., Asokan, K., Kumar, H., Pal Singh, J., Negi, P., & Srivastava, R. C. (2014). FT-IR and Electrical Study of Dysprosium Doped Cobalt Ferrite Nanoparticles. *Journal of Nano science*, 10.
- [26] Valenzuela, R. (2012). *Novel Applications of Ferrites*. *Physics Research International*. Zhukov: Hindawi Publishing Corporation.
- [27] Khanduri, H. (2013). *Magnetic Properties of Functional Oxides*. PhD Dissertation. Tallinn University of Technology, Estonia.
- [28] Chuan, Z. T., Huai Wu, Z., Hua, S., Jie, L., Liang Z. Z., & Yang, L. (2013). Development and application of ferrite materials for low-temperature Co-fired ceramic technology. *Review of magnetism, magnetic materials, and interdisciplinary research*, 22(11), 21.
- [29] Ogsen, G. (2015). *Magneto-optical thin films for magnetic fields visualization*. PhD Dissertation. National academy of sciences of the Republic of Armenia institute of radio physics and electronics, Ashtarak.
- [30] Heilmann, E.L., & Verwey, E.J.W. (1947). Physical Properties and Cation Arrangement of Oxides with Spinel Structures I. Cation Arrangement in Spinel. *Journal of Chemical Physics*, 15, 174-180.

- [31] Angelakeris, M., Kalogirou, O., Makridis, A., Sakellari, D., Simeonidis, K., Topouridou, K., Tziomaki M., Yavropoulou, P. M., & Yovos, G. J. (2014). In vitro application of Mn-Ferrite nanoparticles as novel magnetic hyperthermia agents. *Journals of material chemistry*, 2, 8390-8398
- [32] Cui, J. H., Fu, L. M., Shi, W. J., & Yuan, B. (2013). Synthesis of porous magnetic ferrite nanowires containing Mn and their application in water treatment. *Journals of material chemistry*, 2, 5902-5907.
- [33] Aliabadi, A., Moghaddam, F.M., & Tavakoli, G. (2015). Application of nickel ferrite and cobalt ferrite magnetic nanoparticles in C–O bond formation: a comparative study between their catalytic activities. *Journal of Research and Science advances* 5, 59142–59153.
- [34] Srivastava, R. & Yadav, B. C. (2012). *Ferrite materials: Introduction, synthesis techniques, and applications as sensors*. International PhD of Green nanotechnology, 16.
- [35] Manorama, S. V., Reddy, K. M., & Satyanarayana, L. (2013). Synthesis of nanocrystalline $Ni_{1-x}Co_xFe_{2-x}O_4$: a material for liquefied petroleum gas sensing. *Journal of sensor & actuators*, 89, 62-69.
- [36] Byrappa, K., Kashinath, L., Namratha, K., Srikantaswamy, S., & Vinub, A. (2017). Microwave treated sol–gel synthesis and characterization of hybrid ZnS–RGO composites for efficient photo degradation of dyes. *New Journal of chemistry*, 41, 1723.
- [37] Danks, A., Hall, S., & Schnepf, Z. (2016). The evolution of 'sol-gel' chemistry as a technique for materials synthesis. *Journal of materials horizons*, 3(2), 91-112.
- [38] Mohamed, A., Mohamed, A. M. A., Reddy, M. P., & Shakoor, R. A. (2017). Auto combustion synthesis & magnetic characteristics of Nickel ferrite nanoparticles. *Indian journal of science and technology*, 10(13), 5.
- [39] Mezinskis, G., & Sutka, A. (2012). Sol-gel auto-combustion synthesis of spinel-type ferrite nanomaterials. *Journal of Material Science*, 6(2), 128–141.
- [40] Vijayanand, S. (2010). *Synthesis and characterization of spinel-type magnetic and non-magnetic oxide nanomaterials*. PhD Dissertation. University of Pune, India.

- [41] Bilton, M., Brown, A. P., & Milne, S. J. (2012). Comparison of Hydrothermal and Sol-Gel Synthesis of Nano-Particulate Hydroxyapatite by Characterization at the Bulk and Particle Level. *Open Journal of Inorganic Non-metallic Materials*, 2, 1-10.
- [42] He, M.H., Jiao, D.L., Liu, Z.W., Meng, Y.Y., Ramanujan, R.V., Shukla, S., & Zeng, Q. (2014). Comparison of Hydrothermal and Sol-Gel Synthesis of Nano-Particulate Hydroxyapatite by Characterization at the Bulk and Particle Level. *Journal of Alloys and Compounds*, 583, 220–225.
- [43] Foroutan, F. (2015). *Sol-gel synthesis of phosphate-based glasses for biomedical applications*. PhD Dissertation. University of London, London.
- [44] Mezinskis, G., Pludons, A., & Shutka, A. (2010). Preparation of dissimilarly structured ferrite compounds by sol-gel auto combustion method. *Journal of chemical technology*, 1(54), 6.
- [45] Gonjal, J. P., Morán, E., & Schmid, R. (2015). Microwaves: Microwave Assisted Hydrothermal Synthesis of Nanoparticles. *Journal of Nanotechnology*, 561-570.
- [46] Peng, L. M., Sun, W. T., & Xia, H. R. (2013). Hydrothermal Synthesis of Organometal Halide Perovskites for Li-ion Batteries. *Journal of royal society of chemistry*, 1-3.
- [47] Foroughi, M. R., Monshi, A., & Monshi, M. R. (2012). Modified Scherrer Equation to Estimate More Accurately Nano-Crystallite Size Using XRD. *World Journal of Nano Science and Engineering*, 2, 154-160.
- [48] Alimuddin, Bato, K. M., Kumar, S., & Lee, C. G. (2009). Influence of Al doping on electrical properties of Ni–Cd Nano ferrites. *Journal of Current Applied Physics*, 9, 826–832.
- [49] Saija, K. G. (2012). *Synthesis and Characterization of Tetravalent Cation Substituted Mn-Zn Ferrite Suitable for High Frequency Applications*. PhD Dissertation. University of Saurashtra, Rajkot, India.
- [50] Cheeptham, N., Friedman, C. R., Mason, C., Randhawa, A., & Watson, K. (2016). Using scanning electron microscopy to study microbial communities in speleothem samples collected from Iron Curtain Cave. *Journal of Experimental Microbiology & Immunology*, 2, 1-7.

- [51] John Wiley & Sons (2015). *Energy Dispersive Spectroscopy* (2nd ed.). Southern Gate: Atrium.
- [52] Hanley, Q. S. (2013). Fourier Transforms Simplified: Computing an Infrared Spectrum from an Interferogram. *Journal of Chemical Educ.*, 89 (3), 391–396
- [53] Dhanarajua, R., Rajua, M. K., Brahmajiraob, V., & Bangarraju, S. (2012). Verwey's Hopping Transition Mechanism in relation to Dielectric studies of Zn & Sb substituted Cu ferrites. *International Journal of Science and Technology*, 1(5), 275-285.
- [54] Basu, A., & Prasad A. (2013). Dielectric and impedance properties of sintered magnesium aluminum silicate glass-ceramic. *Journal of Advanced Ceramics*, 2(1), 71–78
- [55] Ashraf, I. M., Badr, A. M., & Elshaikh, H. A. (2011). Impacts of temperature and frequency on the dielectric properties for insight into the nature of the charge transports in the Ti₂S layered single crystals. *Journal of Modern Physics*, 2, 12-25.
- [56] Ali, M. A., Akhter, S., Chowdhury, F. U. Z., Khan, M. N. I., & Uddin, M. M. (2015). Structural properties, Impedance spectroscopy and Dielectric spin relaxation of N-Zn ferrite synthesized by double sintering technique. *The Journal of Materials Science division*, 1-7.